

**NASA
Technical
Paper
2197**

December 1983

NASA
TP
2197
c.1

**The Compressible Aerodynamics
of Rotating Blades Based
on an Acoustic Formulation**

0067803



TECH LIBRARY KAFB, NM

Lyle N. Long

LOAN COPY: RETURN TO
AFWL TECHNICAL LIBRARY
KIRTLAND AFB, N.M. 87117



25th Anniversary
1958-1983



**NASA
Technical
Paper
2197**

1983

The Compressible Aerodynamics of Rotating Blades Based on an Acoustic Formulation

Lyle N. Long

*The George Washington University
Joint Institute for Advancement of Flight Sciences
Langley Research Center
Hampton, Virginia*

NASA

National Aeronautics
and Space Administration

Scientific and Technical
Information Branch

SUMMARY

The purpose of this study was to obtain a theoretical formulation for the pressure on the surface of an arbitrary body moving subsonically through a compressible fluid and to implement the formulation numerically. Important applications exist in the areas of propeller, helicopter, and wing theory.

Farassat has derived a solution to the Ffowcs Williams-Hawkings equation that describes the acoustic pressure due to an arbitrary body in motion. This solution has been very useful in calculating noise due to propellers and helicopters. It is a solution to the inhomogeneous wave equation using the Green's function approach where sources are distributed over the surface of the body. The pressure on the surface of the body is assumed known.

As is typical of integral solutions formulated using the Green's function, the solution developed by Farassat must be carefully interpreted on the surface of the body. The proper way to obtain the governing equation for the surface pressure is to integrate exactly over a small region of the body, take the limit as the "observer" approaches the surface, and then let the size of the region vanish. This procedure is well-known for a doublet distribution and the Kirchhoff-Helmholtz equation. As part of this study, this procedure was carried out for Farassat's equation, a non-trivial problem since the integral is over a body in three-dimensional space and time. The doublet distribution and the Kirchhoff-Helmholtz equation can be shown to be special cases of the resulting integral equation.

The integral equation for the surface pressure is amenable to standard numerical integration techniques, but special precautions must be taken in the vicinity of the singularity on the surface of the body. By breaking the surface into N regions and using quadrature over these regions, one obtains a linear algebraic equation. Repeating this procedure for the observer at N distinct points gives a system of linear equations, whose solution yields the pressure at each of the N points. These pressures can then be used as inputs to Farassat's equation to find the noise due to the body or to find the lift and drag.

The above technique resembles well-known panel methods of aerodynamics (e.g., Smith and Hess's method) except that compressibility effects are accounted for exactly via retarded time without recourse to the Prandtl-Glauert rule. This is important since the rule is only valid for two-dimensional or axisymmetric flows. Since the governing (integral) equation for surface pressure has been determined, the present method is a direct method, in contrast to most panel methods where sources and doublets are distributed over the body and their strengths determined numerically. Another advantage of this technique over more conventional panel methods is that it uses the pressure as the dependent variable. These quantities are continuous across the wake, unlike the velocity potential. Therefore, there is no need to approximate the wake's location or assume a distribution of sources over it.

A computer program has been written to implement the above-described theoretical formulation for arbitrary bodies in rectilinear and/or angular motion. Numerical results have been obtained for the surface pressure distribution on ellipsoids, wings, and helicopter rotors. The agreement between these results and those from other theoretical techniques and experiments has been good even for lifting bodies.

CONTENTS

SUMMARY iii

CONTENTS v

FIGURES vi

SYMBOLS vii

I. INTRODUCTION 1

 A. Motivation 2

 B. Ffowcs Williams-Hawkings (FW-H) Equation 5

 C. Farassat's Solution to FW-H Equation 9

II. ANALYSIS 10

 A. Singular Integrals and Boundary Solutions 10

 B. Integral Equation Without Derivative 13

 C. Integral Equation Valid on Body Surface 15

 D. Reduction to Incompressible Aerodynamics 24

III. COMPUTATIONAL METHOD 25

 A. Approximating Body by a Finite Number of Panels 25

 B. Quadrature Formulas 27

 C. Jacobians and Mapping of Elements 30

 D. Retarded Time Calculation 32

 E. Computer Program 34

IV. LIFTING BODIES 38

V. RESULTS 45

 A. Prolate Ellipsoids 45

 B. Finite Wing 49

 C. Helicopter Rotor Blade 51

VI. CONCLUSION 60

APPENDIX A - LEGENDRE-GAUSS QUADRATURE FORMULAS 61

APPENDIX B - FLOWCHART OF SUBROUTINES IN COMPUTER PROGRAM 62

REFERENCES 63

FIGURES

Figure	Page
1.- ϵ -region of arbitrary body	15
2.- Geometry near singularity in retarded time	17
3.- Body approximated by panels	26
4.- Geometry near singularity in incompressible flow	28
5.- Comparison of Legendre-Gauss quadrature and exact integration for sample integral	29
6.- Velocities and position vectors used in retarded time calculations	32
7.- Computer program flowchart, part I	34
8.- Computer program flowchart, part II	35
9.- Proper order of input coordinate points	36
10.- Numbering of elements	36
11.- Simple six-element airfoil with element numbers	39
12.- Profile of simple six-element airfoil	40
13.- Pressure distribution on simple six-element airfoil	41
14.- Pressure distribution on simple six-element airfoil when $\alpha = 10^\circ$	42
15.- Pressure distribution on simple six-element airfoil when $\alpha = 10^\circ$ with Kutta condition	43
16.- Paneling used to model 5-percent-thick ellipsoid	46
17.- Pressure distribution on 5-percent-thick ellipsoid	46
18.- Paneling used to model 10-percent-thick ellipsoid	47
19.- Pressure distribution on 10-percent-thick ellipsoid	47
20.- Paneling used to model 25-percent-thick ellipsoid	48
21.- Pressure distribution on 25-percent-thick ellipsoid	48
22.- Paneling used to model NACA 0008 wing	49
23.- Pressure distribution on NACA 0008 wing	50
24.- Planform view of paneling used to model NACA 0012 helicopter rotor	51
25.- Paneling used to model NACA 0012 helicopter rotor	51
26.- Pressure distribution on NACA 0012 rotor at 94 percent span when $\alpha = 0^\circ$	53
27.- Pressure distribution on NACA 0012 rotor at 98 percent span when $\alpha = 0^\circ$	54
28.- Pressure distribution on NACA 0012 rotor at 99.5 percent span when $\alpha = 0^\circ$	55
29.- Pressure distribution on NACA 0012 rotor at 94 percent span when $\alpha = 6.18^\circ$	56
30.- Pressure distribution on NACA 0012 rotor at 98 percent span when $\alpha = 6.18^\circ$	57
31.- Pressure distribution on NACA 0012 rotor at 99.5 percent span when $\alpha = 6.18^\circ$	58
32.- Pressure distribution on NACA 0006 rotor at 94 percent span for several tip Mach numbers when $\alpha = 0^\circ$	59

SYMBOLS

a	integration limit for downwash integral
a_{ij}	element of matrix that multiplies vector of discrete pressures from system of algebraic equations ($a_{ij}c_{p_i} = b_i$)
b	integration limit for downwash integral
b_i	element of vector of inhomogeneous terms from system of algebraic equations ($a_{ij}c_{p_i} = b_i$)
b_i'	vector of inhomogeneous terms b_i after applying Kutta condition
c	speed of sound
c_p	pressure coefficient $p/(\rho_0 V^2/2)$ where V is some characteristic velocity
c_{p_i}	pressure coefficient on i th panel
$f(\vec{x}, t)$	function describing body surface
$f_\epsilon(\vec{x}, t)$	function describing ϵ -region of body surface
$f(\xi)$	integrand of downwash integral
f_i	finite element shape functions
$F(x, y)$	downwash integral
$H(f)$	Heaviside function
H_i	Legendre-Gauss weight coefficient for i th node
$\hat{i}, \hat{j}, \hat{k}$	orthogonal unit vectors
$ J $	Jacobian of transformation
k	index used for quadrature node
K_p	kernel for pressure integral
K_R	regular kernel
K_S	singular kernel
K_V	kernel for velocity integral
M	Mach number
M_n	Mach number in normal direction, $\vec{v} \cdot \hat{n}/c$
M_r	Mach number in propagation direction, $\vec{v} \cdot \hat{r}/c$
\dot{M}_r	derivative of Mach number in propagation direction, $\left(\frac{\partial}{\partial \tau} \vec{M}\right) \cdot \hat{r}$

M_t	Mach number in tangential direction, $\sqrt{M^2 - M_n^2}$
\hat{n}	unit normal vector
n_i	ith component of surface normal vector \hat{n}
N	number of elements used to represent body
p	perturbation pressure
p_i	pressure on ith element (observer element)
p_j	pressure on jth element (source element)
P_{ij}	viscous stress tensor
r	$= \vec{r} $
\vec{r}	vector distance between source and observer, $\vec{x} - \vec{y}(\tau)$
\hat{r}	$= \vec{r}/r$
\vec{r}_o (x_o, y_o, z_o)	} observer position vector used in retarded time calculations (fig. 6)
\vec{r}_s (x_s, y_s, z_s)	
R, R'	radial distances on body surface (fig. 2)
R_s	$= \sqrt{x_s^2 + y_s^2}$
Ratio	$= [\cos \theta / r^2 (1 - M_r)^3]_{ret} dS$
t	observer time
T_{ij}	Lighthill's stress tensor, $\rho u_i u_j + P_{ij} - c^2(\rho - \rho_o)\delta_{ij}$
u_i	perturbation fluid velocity (ith component)
u_n	perturbation velocity of fluid in n-direction, $\vec{u} \cdot \hat{n}$
U	rectilinear velocity of body
\vec{v}	velocity of body
v_i	ith component of \vec{v}
v_n	normal velocity of body
v_{n_i}	normal velocity of ith element of body
v_r	surface velocity in propagation direction, $\vec{v} \cdot \hat{r}$

x/c	nondimensional distance from leading edge of airfoil
\vec{x}, x_i	observer position in frame fixed to undisturbed fluid medium
\vec{x}_0	location of observation point \vec{x} when it is on the body at time $t = 0$
\vec{y}, y_i	source position in frame fixed to undisturbed fluid medium
$\vec{y}(\tau)$	location of source in motion
α	angle of attack
β	$= \sqrt{1 - M^2}$
β_n	$= \sqrt{1 - M_n^2}$
β_t	$= \sqrt{1 - M_t^2}$
γ, γ'	angles on surface in ϵ -region (fig. 2)
δ	distance of source from body in normal direction
$\delta(f)$	Dirac delta function
δ_{ij}	Kronecker delta
ϵ	size of hole removed from integral
ϵ_1, ϵ_2	units indicating size of hole removed from downwash integral (section II.A)
$\vec{\zeta}, \zeta_i$	local coordinate system on panel (fig. 4)
$\vec{\eta}, \eta_i$	coordinate system into which panel is transformed for quadrature
η	transformation used in ϵ -region, $\beta_n^2 y - M_n M_t \delta$
η_1	limit of integration, $-\beta_n^2 \epsilon - M_n M_t \delta$
η_2	limit of integration, $\beta_n^2 \epsilon - M_n M_t \delta$
θ	$\arccos(\hat{n} \cdot \hat{r})$
ξ	transformation used in ϵ -region, $\beta \beta_n x$
ξ_2	limit of integration, $\beta \beta_n \epsilon$
ρ	perturbation density
ρ_0	density of the undisturbed medium
τ	retarded time (time of emission), $t - (r/c)$
ϕ	angle used in ϵ -region (fig. 2)
ω	magnitude of angular velocity of body

$\vec{\omega}$ angular velocity of body

Ω_r $(\vec{\omega} \times \hat{n}) \cdot \hat{r}$

Subscript:

ret expression is evaluated at retarded time, $\tau = t - r/c$

Notation:

$\text{sgn}(\delta)$ $\delta/|\delta|$

\oint integration with a specific hole removed from region of integration

\square^2 wave operator

I. INTRODUCTION

In the last few decades, renewed interest in rotating blade technology, specifically in propellers and helicopters, has reversed a decline in propeller development that began in the 1940's with the advent of gas turbines. Since turbojets, and later turbofans, offered significant improvements in reliability, weight, and speed propellers were relegated to only a few specific applications. The low price of fuel allowed the pursuit of higher and higher speeds. However, the rapid increase in fuel costs in the early 1970's changed the equation for direct operating costs, and therefore the effectiveness of all forms of transportation had to be reevaluated. It was soon realized that propellers could be more efficient than turbofans, even at relatively high speeds (up to $M = 0.8$ cruise (ref. 1)).

In the future, highly swept multibladed propellers (propfans) will improve propulsive efficiency by 15 to 22 percent over advanced turbofans (at $M = 0.7$ to 0.8), even after gear and turbine losses. At lower speeds, the propulsive efficiency of propellers is already nearly 90 percent. The propeller definitely has a place as a propulsion device of the future.

Helicopters represent a completely different application of rotating blades. They have become more and more popular, but for reasons other than efficiency. Their main advantage is their ability to land in small areas, which often eliminates the need for ground transportation from the landing pad to the destination. This ground travel time can be significant, since most airports are far from city centers. Including travel from city to airport, an airplane trip from London to Paris requires 160 minutes; the same trip by helicopter requires 70 minutes (ref. 2).

Helicopters satisfy many requirements of communities, businesses, and the military. They are being used to deliver patients to hospitals when time is critically important, and they assist in law enforcement, forestry, and traffic monitoring. Even relatively small corporations can afford helicopters to rush employees from place to place. However, the largest demand for helicopters comes from the military for rescue, reconnaissance, and antitank roles. In addition, they are performing many tasks formerly done by trucks, including hauling airplanes, trucks, and tanks. Of primary importance is their role in rescuing; during the Korean War, helicopters transported over 23 000 casualties, over half of which would have otherwise died (ref. 2).

With renewed interest in rotating blade technology, there is a concomitant interest in the acoustic and aerodynamic characteristics of rotating blades. Despite many advances in aeroacoustics, relatively little has been accomplished in developing efficient aerodynamic methods for propellers and helicopters. The present work presents a compressible aerodynamic method that is especially useful for rotating blades. Specifically, an integral equation governing the pressure on the surface of an arbitrary body is developed, and a finite element numerical procedure (panel method) is used to solve it. The theory is linear and inviscid, and the dependent variable is the pressure, which is governed by the wave equation.

A. Motivation

The present study was motivated by a need for effective noise prediction methods for moving bodies, especially rotating blades. There are several formulations for the noise due to moving bodies (ref. 3). The governing partial differential equations and boundary conditions are usually reduced to integral formulations using the Green's function. These formulations describe the pressure in terms of integrals over the surface of the body, and the surface pressure is contained in the integrands of these equations. Therefore, detailed surface pressure data are required to calculate the noise.

Currently the required surface pressure data can be obtained in several different ways. In some cases, blade element theory is used with standard aerodynamic corrections for compressibility. In others, experimental measurements are used. Whatever the technique, surface pressure is usually obtained via standard aerodynamic methods that were developed before the advent of high-speed computers.

The present work shows that the surface pressure can be calculated from the same integral formulations that govern the acoustics. However, in this case, instead of having an integral representation, one obtains an integral equation, specifically a singular, inhomogeneous Fredholm integral equation of the second kind.

The key word above is singular. Without this complication, there would be few difficulties. Singular integral equations are ambiguous unless interpreted properly. This interpretation forms much of this report and is discussed in detail in section II. In fact, the main contribution of the present work is to derive the governing integral equation for surface pressure and to solve it for several different bodies using a panel method.

By using the acoustic formulation to determine surface pressures and thus eliminating the need for ad hoc aerodynamic methods or experiment, the entire noise prediction methodology for moving bodies becomes autonomous. Also, as progress is made in modeling more and more aspects of the actual flow, they can be included both in surface pressure calculations and in noise calculations simultaneously. In addition, by using the same theory to predict aeroacoustics and aerodynamics, one may be able to develop a deeper understanding of the two phenomena.

The acoustic formulations presented herein were originally suggested by Lighthill based on the acoustic analogy (refs. 4 and 5). Ffowcs Williams and Hawkings (ref. 6) expanded this concept to include the effects of solid surfaces by writing the governing equations of fluid mechanics in the form of an inhomogeneous wave equation (in terms of pressure or density). The inhomogeneities represent boundary conditions, nonlinearities, and viscous effects.

Using the free-space Green's function, one can derive an integro-differential equation from the acoustic analogy. This equation does not represent a solution per se, but for numerical purposes it makes the problem more tractable. Farassat (refs. 7 and 8) has reduced this differential integral formulation to strictly an integral formulation, which is even more amenable to numerical treatment because the need for numerical differentiations is eliminated. Farassat's equation forms the starting point of the present analysis.

Using the acoustic analogy approach implies that the pressure (or density) is the dependent variable. In linearized theory the pressure is proportional to the acceleration potential, as originally discussed by Prandtl in 1936 (ref. 9). Since

then others have used the pressure, or acceleration, method, notably Küssner (ref. 10) and Kondo (ref. 11) and, more recently, Van Holten (ref. 12) and Dat (ref. 13). Since the present effort was motivated by the desire for efficient noise prediction methods, working in the pressure formulation is natural. There was no interest in the details of the wake, the downwash, or the trailing vortices except in how they affect the pressure and normal fluid velocity on the surface. A major advantage in using this formulation as opposed to using the velocity potential is that there is no need to integrate over the wake. Since the pressure, unlike the velocity potential, is continuous across the wake, there are no integrals over the surface of the wake. Of course, the effects of the wake and trailing vortices must be accounted for. This is discussed in section IV.

Linearized acoustics and linearized compressible aerodynamics are one and the same. They both derive from a small perturbation of the continuity and Euler equations, which can be combined to give the wave equation. The link between acoustics and aerodynamics is exploited in few works as much as it is here, however. Generally, acoustics is concerned with the signal after it has radiated from the body. Aerodynamics is concerned with determining the forces on the body. In the current work, both effects are shown to originate from the same phenomenon. Just as one can find the pressure on a vibrating piston using the Kirchhoff-Helmholtz (ref. 14) integral equation, the pressure on the surface of any (thin or slender) moving body can be determined using Farassat's equation.

As already mentioned, linearized compressible aerodynamics is governed by the wave equation; for two-dimensional or axisymmetric bodies in steady, rectilinear motion, the problem is simplified considerably. With the Prandtl-Glauert transformation, the wave equation can be transformed into the Laplace equation, so that one can use the well-known and powerful methods of potential theory. For finite bodies undergoing very complicated motions such as spinning, vibrating, and translating, the problem is not so simple. One has no alternative but to solve the wave equation.

In the past, compressibility corrections developed for two-dimensional bodies in rectilinear motion were used when solving for the aerodynamics of rotating blades. The blade was divided into sections along the span and each section treated as though it were in rectilinear motion with Prandtl-Glauert or Karman-Tsien corrections for compressibility. Although there are more appropriate techniques such as the Goldstein-Lock method (refs. 15 and 16), these do not apply to helicopter blades in forward flight and they also require corrections for compressibility. The method presented herein represents an actual solution to the governing equation, the wave equation. Compressibility, three-dimensionality, and complicated motions are treated together in a unified fashion.

Using the wave equation directly means that the problem is four-dimensional, in space and time. In the past this was a serious obstacle, but today with high-speed computers it is not. In fact, once one becomes accustomed to the notion of four dimensions, the physics becomes much more understandable.

Compressibility manifests itself via a finite propagation speed of disturbances. In this work, compressibility effects are accounted for by considering this finite propagation speed. The time of propagation, or the distance the signal actually travels, is calculated exactly. In rectilinear motion this calculation is completely equivalent to the Prandtl-Glauert transformation, which "stretches" the body to account for the actual distance the signal travels. Because the body and the signal are moving, the signal must travel farther from one point on the body to another. In the current work by using four dimensions and the wave equation, the effect is

accounted for exactly for arbitrary motions. Compressibility is discussed later in terms of retarded time, which has also been used by Küssner (ref. 10), Kondo (ref. 11), Van Holten (ref. 12), Dat (ref. 13), and Morino (ref. 17).

After the integral equation governing the surface pressure is derived, the numerical technique used to solve it is discussed. The computational method can be classified as a finite element technique (ref. 18), but it is more accurately called a panel method. Throughout this work the words element and panel are used interchangeably. In a panel method, the surface of the body is approximated by a finite number of quadrilaterals and the pressure is assumed to follow some given behavior over each element; in this case it is assumed to be constant over each element.

The numerical approach used here can also be classified as a boundary integral equation (BIE) method (ref. 19) which has become very popular in the last few decades. This method has been used in several different fields including fracture mechanics (ref. 20), potential theory (refs. 21 and 22), structures (ref. 23), and acoustics (refs. 24 and 25). The advantage of these methods is that the problem is reduced from one in space to one over a hypersurface.

Probably the most common examples of BIE or panel methods are the aerodynamic codes of Hess and Smith (refs. 26 and 27). Their codes were originally designed to solve for the velocity potential on nonlifting bodies in rectilinear motion (ref. 28) and later were expanded to include the effects due to lift (ref. 29). The governing integral equation is that given by Lamb (ref. 30) as the Green's function formulation of the Laplace equation. This is essentially a distribution over the surface of the body and the wake of sources and doublets whose strengths are adjusted to satisfy the appropriate boundary conditions. Numerous other very effective panel methods exist, notably MCAIR (ref. 31), MBB (ref. 32), PANAIR (ref. 33), and NLR (ref. 34), which were developed by McDonnell Douglas, Messerschmitt-Bolkow-Blohm, Boeing, and the Netherland's National Aerospace Laboratory, respectively.

Panel methods have been very effective for aircraft configurations, but they are not suitable for rotating blades because they use two-dimensional compressibility corrections (Prandtl-Glauert, Göthert, or Karman-Tsien rules (refs. 35 and 36)) and they assume rectilinear motion. Furthermore, these methods are all too complicated to justify using them to calculate the inputs (surface pressures) to an acoustics prediction program. They would be much too costly to adapt and to run. The efficiency of the present formulation supports this claim.

Another panel method, developed by Morino (refs. 17 and 37), does account for compressibility in terms of retarded time. This method is an inviscid velocity-potential formulation in contrast to the present pressure formulation. As discussed earlier, one must integrate over the wake when the velocity potential is the dependent variable. Furthermore, Morino's method results in a convected wave equation because the frame of reference is not fixed to the undisturbed fluid. Apparently he foresaw mainly aircraft-type applications for this work and thus the emphasized rectilinear motion. The integral equation thus acquires a very complicated form that would seem to limit its utility in clarifying the physics of the problem (see eq. 1.5, ref. 17). In addition, although both the present method and Morino's method (SOUSSA-P 1.1 (ref. 38)) have been programmed for the case of linearized theory and both could be expanded to include nonlinear effects, the present method could also be expanded to include viscous effects (since viscosity is already included in the Ffowcs Williams-Hawkings (FW-H) equation).

Another important point regarding the method of reference 17 concerns the treatment of the singularity in the integral equation. This treatment is also referred to as interpreting the equation, regularizing the equation, or putting the observer on the surface and is performed in section II.C of the present work. Although Morino criticizes Widnall's method because it requires a Cauchy principal value interpretation, Morino does not state that his method could also be classified as such. In fact, so could all surface singularity methods, including the present one. This leads to the questions of how one treats the singularity and the meaning of the Cauchy principal value. In this report the singularity is treated analytically and its relation to the Cauchy principal value is demonstrated. Morino claims to have done this also (using a velocity-potential formulation), but the results seem to differ from those presented here. All of this is discussed in section II.C.

The remainder of section I is devoted to presenting the FW-H equation and one of Farassat's solutions to it. For completeness, the linearized version of the FW-H equation is derived. These sections also illustrate the importance of generalized function theory (ref. 39).

B. Ffowcs Williams-Hawkings (FW-H) Equation

The Ffowcs Williams-Hawkings (FW-H) equation is

$$\square^2 p = \frac{\partial}{\partial t} [\rho_0 v_n |\nabla f| \delta(f)] - \frac{\partial}{\partial x_i} \left[p_{ij} \frac{\partial f}{\partial x_j} \delta(f) \right] + \frac{\partial^2 [T_{ij} H(f)]}{\partial x_i \partial x_j} \quad (1)$$

where \square^2 signifies the wave operator,

$$\square^2 p = \frac{1}{c^2} \frac{\partial^2 p}{\partial t^2} - \nabla^2 p$$

This equation was first derived in reference 6. Farassat also derived it in reference 8 using a method called embedding. It represents a combination of the mass continuity and conservation of momentum equations, plus the boundary conditions.

The first term on the right hand side of equation (1) behaves like a monopole. It represents the normal velocity boundary condition. One can envisage this as a distribution of mass sources. Often called the "thickness" term, it is shown subsequently to be the equivalent to the thickness terms used in linearized aerodynamics.

The second term behaves like a dipole distribution and is due to the viscous stresses and thermodynamic pressures acting on the surface.

The last term on the right hand side is the quadrupole term. It contains the nonlinear effects, such as turbulence. In Lighthill's work (ref. 5), this was the only term on the right hand side, but it is usually considered unimportant for noise due to moving bodies. However, preliminary studies recently conducted indicate that

these terms can be significant in the transonic and high supersonic speed regimes for thin wedge-shaped airfoils (refs. 40 and 41).

The FW-H equation is easily derived from the governing equations of fluid mechanics using the embedding procedure (ref. 8). This procedure converts the problem into one in unbounded space. The boundary conditions become source terms, so that the free-space Green's function can be used. A simple example is given in reference 8. Converting boundary conditions to sources is not uncommon and is discussed in reference 42 (pp. 791-792).

Throughout this study only the linearized version of the FW-H equation is used; thus, for completeness this version is derived. The small perturbation forms of the governing equations of fluid mechanics are

$$\frac{1}{c^2} \frac{\partial p}{\partial t} + \rho_0 \frac{\partial u_i}{\partial x_i} = 0 \quad (2)$$

$$\rho_0 \frac{\partial u_i}{\partial t} + \frac{\partial p}{\partial x_i} = 0 \quad (3)$$

$$p = c^2 \rho$$

where all terms higher than first order are neglected and the summation convention is implied. These are also referred to as the linear acoustic equations. Their range of validity is discussed in reference 14.

If the derivatives are interpreted as generalized derivatives (refs. 39 and 43) and the field variables are defined as generalized functions, then the possibility of finite jumps in these variables (e.g., across surfaces and shocks) must also be included in these equations. If one considers only subsonic flow, the only discontinuity surface is the body and the wake. It is easily shown that the governing equation for the pressure has no contribution from the wake. If one is interested in the velocity potential, the wake must be considered. In this report the wake is not even included because the result would be unchanged if it were.

Interior to the body the acoustic quantities are assumed equal to zero. This is arbitrary, however, and for other problems it may be advantageous to assume some other value. The procedure is carried out formally by writing all the flow quantities multiplied by a Heaviside function $H(f)$ where $f(\vec{x}, t)$ describes the body surface and $f < 0$ inside the body. As examples, $\partial p / \partial t$ and $\partial p / \partial x_i$ become

$$\begin{aligned} \overline{\frac{\partial p}{\partial t}} &= \frac{\partial p}{\partial t} + [p] \frac{\partial f}{\partial t} \delta(f) \\ &= \frac{\partial p}{\partial t} + p \frac{\partial f}{\partial t} \delta(f) \end{aligned}$$

$$\bar{\frac{\partial p}{\partial x_i}} = \frac{\partial p}{\partial x_i} + p \frac{\partial f}{\partial x_i} \delta(f)$$

where the bars over derivatives denote generalized differentiation. Also, the brackets indicate the jump in that quantity across the surface. Note that inside the body, pressure, density, and fluid velocity perturbations all vanish. The operators of equations (2) and (3) are applied to the generalized quantities as follows:

$$\frac{1}{c^2} \bar{\frac{\partial p}{\partial t}} + \rho_o \frac{\bar{\partial u_i}}{\partial x_i} = \left(\frac{1}{c^2} \frac{\partial p}{\partial t} + \rho_o \frac{\partial u_i}{\partial x_i} \right) + \frac{p}{c^2} \frac{\partial f}{\partial t} \delta(f) + \rho_o u_i \frac{\partial f}{\partial x_i} \delta(f) \quad (4)$$

$$\rho_o \frac{\bar{\partial u_i}}{\partial t} + \frac{\bar{\partial p}}{\partial x_i} = \left(\rho_o \frac{\partial u_i}{\partial t} + \frac{\partial p}{\partial x_i} \right) + \rho_o u_i \frac{\partial f}{\partial t} \delta(f) + p \frac{\partial f}{\partial x_i} \delta(f) \quad (5)$$

The terms in parentheses vanish because of equations (2) and (3). Using the relation (ref. 30)

$$\frac{\partial f}{\partial t} + v_i \frac{\partial f}{\partial x_i} = 0$$

where v_i is the velocity of a point on the body, and noting that the normal to the body is

$$n_i = \frac{1}{|\nabla f|} \frac{\partial f}{\partial x_i}$$

gives

$$\frac{\partial f}{\partial t} = -v_n |\nabla f|$$

Since there is no flow through the body,

$$u_n = v_n$$

Using these relations, equations (4) and (5) become (after eliminating second order terms)

$$\frac{1}{c^2} \bar{\frac{\partial p}{\partial t}} + \rho_o \frac{\bar{\partial u_i}}{\partial x_i} = \rho_o v_n |\nabla f| \delta(f) \quad (6)$$

$$\rho_o \frac{\bar{\delta} u_i}{\partial t} + \frac{\bar{\delta} p}{\partial x_i} = p n_i |\nabla f| \delta(f) \quad (7)$$

Taking the generalized derivative of equations (6) and (7) with respect to x_i and t , respectively, and subtracting yields

$$\bar{\square}^2 p = \frac{\bar{\delta}}{\partial t} [\rho_o v_n |\nabla f| \delta(f)] - \frac{\bar{\delta}}{\partial x_i} [p n_i |\nabla f| \delta(f)]$$

which is the linearized FW-H equation. Terms involving products of small perturbation quantities have been neglected, along with viscous effects. It is well-known that near stagnation points the assumption of small perturbations is not valid, but this affects only a small region around the stagnation point (ref. 44, p. 209).

An important point to make at this time concerns the pressure formulation versus the velocity-potential formulation. The present work uses the pressure as the dependent variable and the flow is linearized from the beginning. In the past it has been more common to use the velocity potential, especially for very low speeds, because at speeds much less than the speed of sound one can assume that the flow is incompressible. In this case the continuity equation becomes

$$\nabla \cdot \vec{u}_t = 0$$

or

$$\nabla^2 \phi = 0$$

where

$$\nabla \phi = \vec{u}_t$$

and ϕ is the velocity potential and \vec{u}_t is the net fluid velocity. Thus the velocity potential is governed by the well-known Laplace equation. More importantly, however, there is no need to assume small perturbations. Thus, for very low speeds and inviscid flow, the problem is relatively easy to solve with all the nonlinearity contained in the Bernoulli equation.

On the other hand, if one begins with the small perturbation theory of equations (2) and (3), the governing equation is the wave equation (on the pressure, velocity, and velocity potential). But at very low subsonic speeds, using the wave equation on the pressure is not as accurate as using the Laplacian on the velocity potential (especially near stagnation points), because the pressure satisfies the Laplacian only for small perturbations. The momentum equation is nonlinear, so that the Bernoulli equation is nonlinear.

The relation between the above theories is somewhat complicated because it involves two different asymptotic expansion procedures. In the small perturbation method one assumes that

$$\rho_t = \rho_o + \epsilon \rho' + \dots$$

$$p_t = p_o + \epsilon p' + \dots$$

$$\vec{u}_t = \epsilon \vec{u}' + \dots$$

where ρ_t and p_t are the net density and pressure, p_o is the pressure of the undisturbed medium, the primes indicate perturbation quantities, and ϵ is a measure of the body thickness. This method becomes exact as the thickness approaches zero. It is often useful away from stagnation points even for relatively thick bodies. In the incompressible problem one assumes that ϵ is a measure of the Mach number. This is exact as $M \rightarrow 0$ for any body and is known to be useful for small but finite Mach numbers (ref. 35).

However, since the main concern here is in rotating blades, which are thin and usually operate at high speeds, the linearized small perturbation theory is appropriate. This formulation will be accurate as long as the disturbances remain small, even at relatively high subsonic Mach numbers. In fact, this formulation gives useful results for supersonic motions also. However, one must then account for multiple emission times. The transonic regime is, of course, inherently nonlinear.

C. Farassat's Solution to FW-H Equation

Farassat has derived several different integral representations of the FW-H equation. Each one is particularly well suited to a different application or numerical solution technique (ref. 45). The one that is most appropriate for the present work is equation (9) of reference 8:

$$4\pi p(\vec{x}, t) = \frac{1}{c} \frac{\partial}{\partial t} \int_{f=0} \left(\frac{\rho_o c v_n + p \cos \theta}{r |1 - M_r|} \right)_{ret} dS + \int_{f=0} \left(\frac{p \cos \theta}{r^2 |1 - M_r|} \right)_{ret} dS \quad (8)$$

where

$$\cos \theta = \hat{n} \cdot \hat{r}$$

$$\hat{r} = \frac{\vec{r}}{r}$$

$$M_r = \frac{\vec{v} \cdot \hat{r}}{c}$$

$$r = |\vec{x} - \vec{y}(\tau)|$$

$$\tau = t - \frac{r}{c}$$

The subscript *ret* signifies that the expression is to be evaluated at retarded time τ . This accounts for compressibility of the flow where the "source" at $\vec{y}(\tau)$ (in motion) emits a signal that arrives at the stationary "observer" at \vec{x} a short time after it is emitted. This is unlike incompressible flow where signals travel with infinite speed. Therefore the integration over the body surface, $f(\vec{x}, t) = 0$, is not carried out at a single emission time τ because different points on the surface have different emission times. Of course, one is only interested in the signals that arrive at \vec{x} at the same time. Note that retarded time is a more common concept in electromagnetic theory than in acoustics or aerodynamics (ref. 46).

It is sometimes useful to consider the retarded time process in reverse order in terms of a collapsing sphere (ref. 8), as Nystrom and Farassat (ref. 45) did in the calculation of the noise due to high-speed propellers.

It should be remembered that equation (8) is not a solution per se, but more accurately a representation. Since the integrals contain the unknown, the pressure on the surface of the body, the problem has not actually been "solved." However, if one knows the surface pressure on a given body, equation (8) predicts the noise due to that body.

Equation (8) represents the starting point for this report. Although it has been effective in predicting noise from bodies in motion, it has not been used to predict surface pressures on arbitrary bodies, mainly because the integrals become singular when the observer is on the surface. A mathematical limiting procedure is required, the details of which are described in the next section.

II. ANALYSIS

A. Singular Integrals and Boundary Solutions

Singular integrals are very common in mathematical physics because of the frequent use of the Green's function technique, which can be thought of as a distribution of singularities or delta functions. Whenever one desires surface information from such a method, singular integrals may arise. These singularities must be interpreted properly to obtain meaningful results, because truly singular integral equations are ambiguous. Usually, however, these integrals are special cases of regular integrals, and their proper interpretation can be inferred from the physics.

Singular integrals are especially common in aerodynamic theory because of the emphasis on surface data. They appear in equations for the velocity potential, the acceleration potential, and the downwash integral, to name a few. They are the basis of the modern panel methods as well as lifting surface and lifting line theories.

Thus the real difficulty in using the acoustic formulation to predict surface pressures is that the integral equation becomes singular if naively interpreted. That is, if \vec{x} is on $f = 0$, then at some point, $\vec{x} = \vec{y}$, which means that $r = 0$. At this point the integrand becomes infinitely large.

The level of difficulty that this fact presents cannot be minimized. Despite tremendous advances in numerical methods, Baker (ref. 47) states:

The impression I intend to convey is that the treatment of singular integral equations is not completely understood at the present....There appear to exist very few effective methods for solving such equations.

The proper way to interpret singular integrals is through a limiting process (refs. 42 and 48 to 50). In the acoustic formulations, one must assume that the observer approaches the surface in the limit from the proper side of the surface (inside or outside depending on the problem being solved). However, this limit must be taken after integrating over the surface, which presents a problem for complicated integrals such as are present here.

As an example of how a singular integral is interpreted, a one-dimensional equation called the downwash integral (ref. 50) is developed. The approach to interpreting this simple equation is essentially the same technique that is used to treat Farassat's equation. The downwash integral is defined as

$$F(x,y) = \int_a^b \frac{f(\xi) (x - \xi) d\xi}{(x - \xi)^2 + y^2} \quad (9)$$

where $F(x,y)$ represents the velocity in a two-dimensional flow due to a distribution of sources and sinks along $a < \xi < b$ of strength $f(\xi)$. When $y = 0$, this integral reduces to the familiar integral

$$\int_a^b \frac{f(\xi) d\xi}{x - \xi}$$

which is commonly defined in terms of a Cauchy principal value technique; that is, a small symmetric region about $\xi = x$ is removed. Quite often this form, with $y = 0$, is the starting point for an analysis. Ordinarily the Cauchy principal value integral, like other singular integrals in higher dimensions, derives from an integral that is not singular, such as the one shown for $F(x,y)$. The surface representation is valid only in the limit, even for the Cauchy principal value, as is now shown.

Strictly speaking, equation (9) is undefined for $y = 0$ when $a < x < b$. The proper way to obtain the value of this integral for $y = 0$ is by taking the limit as $y \rightarrow 0$, but the limiting process must be performed after the integration, that is,

$$F(x,0) = \lim_{y \rightarrow 0} \int_a^b \frac{f(\xi) (x - \xi) d\xi}{(x - \xi)^2 + y^2}$$

Mangler (ref. 50) showed how to derive the Cauchy principal value form, by breaking up the region of integration. That is, write

$$F(x, 0) = \lim_{y \rightarrow 0} \left[\int_a^{x-\varepsilon_1} + \int_{x-\varepsilon_1}^{x+\varepsilon_2} + \int_{x+\varepsilon_2}^b \frac{f(\xi) (x - \xi) d\xi}{(x - \xi)^2 + y^2} \right]$$

where ε_1 and ε_2 are arbitrarily small and of the same order. Now for the regions that do not include $\xi = x$, the integral is well behaved and one can set $y = 0$. Within the ε -region, expanding $f(\xi)$ in a Taylor series about $\xi = x$ gives

$$F(x, 0) = \int_a^{x-\varepsilon_1} + \int_{x+\varepsilon_2}^b \frac{f(\xi) d\xi}{x - \xi} + \lim_{y \rightarrow 0} \frac{f(x)}{2} \ln \left(\frac{\varepsilon_2^2 + y^2}{\varepsilon_1^2 + y^2} \right) + O(\varepsilon)$$

Taking the limit yields

$$F(x, 0) = \int_a^{x-\varepsilon_1} + \int_{x+\varepsilon_2}^b \frac{f(\xi) d\xi}{x - \xi} + f(x) \ln \left(\frac{\varepsilon_2}{\varepsilon_1} \right) + O(\varepsilon)$$

The well-known Cauchy principal value is for an ε -region symmetric about $\xi = x$; thus for $\varepsilon_1 = \varepsilon_2 = \varepsilon$,

$$F(x, 0) = \int_a^{x-\varepsilon} + \int_{x+\varepsilon}^b \frac{f(\xi) d\xi}{x - \xi} + O(\varepsilon)$$

which is the Cauchy principal value.

This integral is correctly termed a semiconvergent integral (ref. 48); that is, for a differently shaped ε -region, a different form of the equation is obtained. For a fully convergent integral, a term like $\ln(\varepsilon_2/\varepsilon_1)$ would not be present and thus the region that was given special treatment would not matter. This point is very important in the subsequent interpretation of Farassat's equation. To fully appreciate and use the principal value concept, one must realize that the region around the singularities cannot simply be deleted. Different ε -regions require different representations. The numerical values of the final results for two different ε -regions are the same though, because any portion the solution left out of the integral shows up in "extra" terms.

In the following section an equivalent procedure is applied to Farassat's equation to obtain an equation valid on the surface of the body. It too is semiconvergent and the form of the extra term that comes from the ε -region depends on the size and shape of the ε -region, just as for the downwash integral of the Cauchy principal value.

B. Integral Equation Without Derivative

Farassat's equation (8) is an integro-differential equation. Taking the derivative inside the integral produces an additional singular integrand, that is, one with $1/r^2$ dependence. Since the main interest here is in the form of the equation on the surface, it is important to bring the derivative under the integral to illuminate the singular term and allow it to be regularized. An integral equation with the derivative inside has been used by Woan and Gregorek (ref. 51) for noise prediction and is presented in a more general form by Farassat (refs. 3 and 7).

The relations necessary to eliminate the derivative are, from Farassat,

$$\frac{\partial}{\partial t} = \frac{1}{1 - M_r} \frac{\partial}{\partial \tau}$$

$$\frac{\partial r}{\partial \tau} = -v_r$$

$$\frac{\partial M}{\partial \tau} = \dot{M}_r + \frac{c}{r}(M_r^2 - M^2)$$

These give

$$\frac{\partial}{\partial \tau} \left[\frac{1}{r(1 - M_r)} \right] = \frac{r\dot{M}_r + c(M_r^2 - M^2)}{r^2(1 - M_r)^2}$$

In addition, one other relation is required. Farassat uses the general stress term $\hat{l}_i \hat{r}_i$ and does not simplify it to the inviscid form $p \hat{n}_i \hat{r}_i = p \cos \theta$. This simplification gives

$$\begin{aligned} \frac{\partial}{\partial \tau} \cos \theta &= \frac{\partial}{\partial \tau} \left(\frac{\hat{n} \cdot \vec{r}}{r} \right) \\ &= \hat{r} \cdot (\vec{\omega} \times \hat{n}) - \frac{v_n}{r} + \frac{v_r \cos \theta}{r} \end{aligned}$$

Defining

$$\Omega_r = \hat{r} \cdot (\vec{\omega} \times \hat{n})$$

gives

$$\frac{\partial}{\partial \tau} \cos \theta = \Omega_r - \frac{v_n}{r} + \frac{v_r \cos \theta}{r}$$

The above relation allows one to write equation (1) without the derivative. It becomes

$$\begin{aligned}
4\pi p(\vec{x}, t) = & \frac{1}{c} \int_{f=0} \left\{ \frac{(\rho_o c v_n + p \cos \theta) [r \dot{M}_r + c(M_r - M^2)]}{r^2 (1 - M_r)^3} \right\}_{ret} dS \\
& + \frac{1}{c} \int_{f=0} \left[\frac{p(r\Omega_r + v_r \cos \theta - v_n)}{r^2 (1 - M_r)^2} \right]_{ret} dS \\
& + \int_{f=0} \left[\frac{p \cos \theta}{r^2 (1 - M_r)} \right]_{ret} dS
\end{aligned}$$

A slightly more general form, which includes unsteady pressures and velocities, is derived in reference 7.

Regrouping these terms into those that do and do not become singular on the surface gives

$$4\pi p(\vec{x}, t) = \int_{f=0} K_R(\vec{x}, t; \vec{y}, \tau) dS + \int_{f=0} K_S(\vec{x}, t; \vec{y}, \tau) dS \quad (10)$$

where

$$\begin{aligned}
K_R = & \left\{ \frac{\rho_o c^2 M_n \dot{M}_r + p \Omega_r (1 - M_r) + p \dot{M}_r \cos \theta}{c r (1 - M_r)^3} \right\}_{ret} \\
K_S = & \left\{ \frac{\rho_o c^2 M_n (M_r - M^2) + p [(1 - M^2) \cos \theta - (1 - M_r) M_n]}{r^2 (1 - M_r)^3} \right\}_{ret}
\end{aligned}$$

For incompressible flow, K_R is clearly a regular integrand because when \vec{x} is on the surface $f = 0$,

$$\frac{1}{r} dS = O(1)$$

Similarly, in incompressible flow, K_S represents the singular portion of the integrand because when \vec{x} is on $f = 0$,

$$\frac{1}{r^2} dS = O\left(\frac{1}{r}\right)$$

and $r = 0$ ($\vec{x} = \vec{y}$) at some point.

C. Integral Equation Valid on Body Surface

In section II.A, a method was described for interpreting a simple semiconvergent integral. The final result was the well-known Cauchy principal value. In this section the same procedure is used to interpret Farassat's equation when the observation point \vec{x} is on the surface $f(\vec{x}, t) = 0$. The equations are lengthy because of the complicated four-dimensional integrands, but the procedure is completely analogous to that already described. As for the downwash integral, Farassat's equation is undefined for $r = 0$ unless it is interpreted properly.

In the case of the downwash integral, the region of integration was divided into one that contained the singularity and one that did not. The integral over the region without the singularity was numerically straightforward to compute. This was not true of the region that contained the singularity, subsequently called a "hole." Therefore, over this hole the integral was treated analytically in such a way that the error could be made arbitrarily small by letting the size of the hole become arbitrarily small. That is, the error was shown to be of the order of the size of the hole. More importantly however, the form of the equation (the extra term) was shown to depend on the shape of the hole. Thus, the integral was semiconvergent. If an asymmetric hole around the singularity were chosen, the Cauchy principal value technique would not apply. For an asymmetric hole one cannot simply neglect the value of the integral over the hole because it has a finite value. This extra term becomes zero when the hole is symmetric.

The first step is to divide the region of integration into two parts, one that includes the singularity and one that does not. For the downwash integral this was done by breaking the ξ -axis into three parts. Farassat's equation is an integral over a surface, so the surface is divided into two parts: one part over the original body surface with a small hole around the singularity removed and the other part over the surface of the hole itself. See figure 1. The combination of these two regions is the original surface, $f(\vec{x}, t) = 0$.

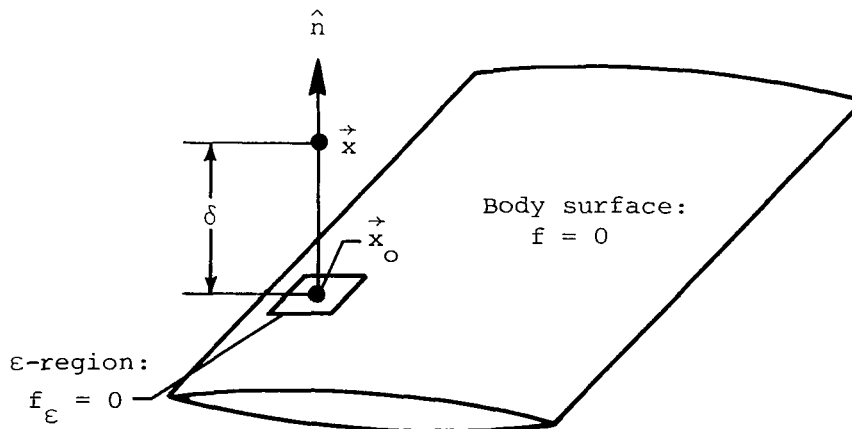


Figure 1.- ϵ -region of arbitrary body.

Thus, Farassat's equation is written

$$4\pi p(\vec{x}, t) = \int_{f=0} K_R(\vec{x}, t; \vec{y}, \tau) dS + \int_{f=0} K_S(\vec{x}, t; \vec{y}, \tau) dS \\ + \int_{f_{\epsilon}=0} K_S(\vec{x}, t; \vec{y}, \tau) dS$$

where f indicates that a specific hole has been removed and f_{ϵ} is the surface of the hole. Note that it is not necessary to break up the region of integration in the regular integral K_R .

The first two integrals present no difficulties numerically since they are both convergent. By definition, neither of them contains a singularity. The third integral is difficult to calculate numerically. The proper way to obtain its form, for an observer located at \vec{x}_o , is via a mathematical limiting process where the observer is located at \vec{x} at a distance of δ above the surface. Then, after integrating, the limit as $\delta \rightarrow 0$ is performed (see fig. 1). This limit is analogous to the limit as $y \rightarrow 0$ in the downwash integral. Note that for convenience \vec{x} is taken to be along the normal to the surface at \vec{x}_o . Mathematically one can write this procedure as

$$p(\vec{x}_o, t) = \lim_{\delta \rightarrow 0} p(\vec{x}, t)$$

Hence the integral equation becomes

$$4\pi p(\vec{x}_o, t) = \int_{f=0} K_R(\vec{x}_o, t; \vec{y}, \tau) dS + \int_{f=0} K_S(\vec{x}_o, t; \vec{y}, \tau) dS \\ + \lim_{\delta \rightarrow 0} \int_{f_{\epsilon}=0} K_S(\vec{x}, t; \vec{y}, \tau) dS \quad (11)$$

The first two integrals can be obtained by simply replacing \vec{x} by \vec{x}_o (setting $\delta = 0$) since they are convergent, but this is not possible in the third integral. One has no alternative but to perform that integration first and then take the limit; otherwise the integral is divergent. However, this integral is too complicated to allow analytic evaluation for most bodies of interest, especially since the integrand K_S contains the unknown pressure p . One would have to solve the entire integral equation and then take the limit as $\delta \rightarrow 0$, to obtain an analytic expression for the surface pressure. Note that in equation (9), the downwash integral example, the procedure leading to the final result was as follows: expand $f(\xi)$ in a Taylor series around $\xi = x$ and obtain an approximate analytic expression for the integral with an estimate of the error.

An analogous approach can be used on Farassat's equation. By assuming that the size of the hole, or ϵ -region, is small, one can approximate the region as planar. In addition, the pressure can be expanded in a Taylor series about the point \vec{x}_o ;

that is, the pressure is assumed to be constant over the ϵ -region. Using these approximations, one can then calculate the third integral in equation (11) analytically and obtain an estimate of the error involved.

The remainder of this section is devoted to obtaining the appropriate analytic expression for the third integral in equation (11). For reasons that will be obvious later, a square is chosen for the shape of the ϵ -region, but the final result is applicable to differently shaped ϵ -regions with a symmetry to be described later.

To perform this integration over a small, square, planar panel, one must first write the integrand K_S in terms of surface coordinates. This is nontrivial because the integrand involves four dimensions (space and time). Figure 2 is an enlarged view of the ϵ -region shown in figure 1. It shows the panel at two different times.

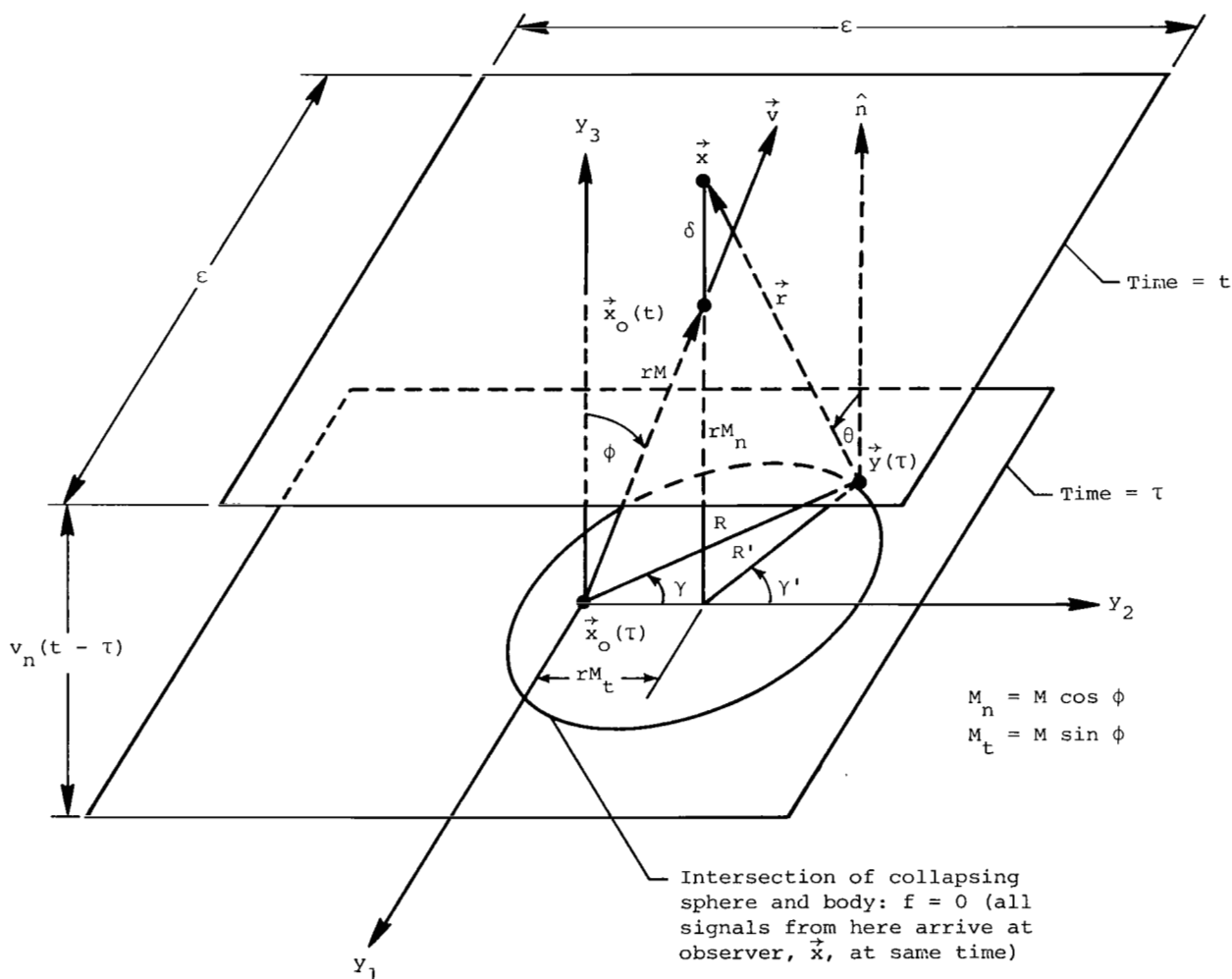


Figure 2.- Geometry near singularity in retarded time.

The time t is the reception time and τ is the emission time. Thus, a signal emitted from the surface point $\vec{y}(\tau)$ at time τ is received at the (stationary) observer point \vec{x} at time t . The δ on this figure is the same δ that was used

on figure 1. The upper plane is the position of the panel at the time t , the time when the observer receives the signal from $\vec{y}(\tau)$. The lower plane is the position of the panel when the signal was emitted. The angle between the surface normal \hat{n} and the radiation direction \vec{r} is θ . For convenience, the coordinate system (fixed to the panel) is aligned so that the panel velocity vector is in the y_1y_2 -plane. The angle between the velocity and the y_3 -axis is defined as ϕ .

As mentioned earlier, the observation point \vec{x} is always stationary. Therefore, when one speaks of the observation point being on the surface, one must specify at what time this occurs. In figure 2, notice that $\vec{x} \rightarrow \vec{x}_o(t)$ when $\delta \rightarrow 0$. This surface point \vec{x}_o is of course moving, but when the time equals t , it is a distance δ away from \vec{x} in the direction of the normal. This means that

$$\vec{x} - \vec{x}_o(t) = \delta \hat{n}[\vec{x}_o(t)]$$

or

$$|\vec{x} - \vec{x}_o(t)| = \delta$$

Figure 2 is useful because many of the quantities on it are known. For example, it is known that $r = c(t - \tau)$ since the distance a signal travels is simply the speed multiplied by the time of propagation. In addition, the distance the panel moves in this time period is $|\vec{x}_o(\tau) - \vec{x}_o(t)|$ which is $v(t - \tau)$. Thus, $rM = v(t - \tau)$.

The purpose of this section is to integrate K_S over the area of this arbitrary panel. By assuming a planar panel, one can simplify K_S considerably. For example, it is obvious that

$$\cos \theta = M_n + \frac{\delta}{r}$$

where $M_n = \vec{v} \cdot \hat{n}/c$. Thus, K_S can be written as

$$K_S = \left\{ \frac{\rho_o c^2 M_n (M_r - M^2) + p[(1 - M^2)(M_n + \delta/r) - (1 - M_r)M_n]}{r^2 (1 - M_r)^3} \right\}_{ret}$$

which can be simplified to

$$K_S = \left[\frac{M_n (\rho_o c^2 + p)(M_r - M^2)}{r^2 (1 - M_r)^3} + \frac{\beta^2 p \delta}{r^3 (1 - M_r)^3} \right]_{ret}$$

Therefore, equation (11) becomes

$$4\pi p(\vec{x}_O, t) = \int_{f=0} K_R dS + \int_{f=0} K_S dS$$

$$+ \lim_{\delta \rightarrow 0} \int_{-\epsilon}^{\epsilon} \int_{-\epsilon}^{\epsilon} \left[\frac{M_n (\rho_o c^2 + p) (M_r - M^2)}{r^2 (1 - M_r)^3} + \frac{\beta^2 p \delta}{r^3 (1 - M_r)^3} \right]_{\text{ret}} dy_1 dy_2 + O(\epsilon)$$

Now assuming that p and \vec{v} are constant over the ϵ -region yields

$$4\pi p(\vec{x}_O, t) = \int_{f=0} K_R dS + \int_{f=0} K_S dS$$

$$+ M_n (\rho_o c^2 + p) \lim_{\delta \rightarrow 0} \int_{-\epsilon}^{\epsilon} \int_{-\epsilon}^{\epsilon} \left[\frac{M_r - M^2}{r^2 (1 - M_r)^3} \right]_{\text{ret}} dy_1 dy_2$$

$$+ p \lim_{\delta \rightarrow 0} \int_{-\epsilon}^{\epsilon} \int_{-\epsilon}^{\epsilon} \left[\frac{\beta^2 \delta}{r^3 (1 - M_r)^3} \right]_{\text{ret}} dy_1 dy_2 + O(\epsilon) \quad (12)$$

All that is required now to integrate equation (12) is to write the integrands in the last two integrals in terms of y_1 and y_2 . From the geometry shown in figure 2 and algebra, the propagation vector \vec{r} can be written in terms of its components in the local coordinate system:

$$\vec{r} = (R' \sin \gamma', -R' \cos \gamma', r \cos \theta)$$

where R' , γ' , and θ are defined in figure 2. Using the relations,

$$R' \sin \gamma' = R \sin \gamma$$

$$R' \cos \gamma' = R \cos \gamma - rM_t$$

$$r \cos \theta = \delta + rM_n$$

which are obtained from geometry, one gets

$$\vec{r} = (R \sin \gamma, rM_t - R \cos \gamma, \delta + rM_n) \quad (13)$$

Therefore the magnitude of \vec{r} is governed by

$$\beta^2 r^2 + 2(RM_t \cos \gamma - \delta M_n)r - R^2 - \delta^2 = 0$$

where

$$\beta^2 = 1 - M^2$$

and

$$M^2 = M_n^2 + M_t^2$$

Using the quadratic formula gives

$$\beta^2 r = (\delta M_n - RM_t \cos \gamma) + \sqrt{(\delta M_n - RM_t \cos \gamma)^2 + \beta^2 (R^2 + \delta^2)} \quad (14)$$

which can be simplified by taking the scalar product of the Mach number vector

$$\vec{M} = (0, M_t, M_n)$$

and \vec{r} (eq. (13)) to get

$$rM_r = M^2 r - RM_t \cos \gamma + \delta M_n \quad (15)$$

Subtracting r from both sides of equation (15) and then multiplying by -1 gives

$$r(1 - M_r) = \beta^2 r + RM_t \cos \gamma - \delta M_n$$

Substituting equation (14) gives

$$r(1 - M_r) = \sqrt{(\delta M_n - RM_t \cos \gamma)^2 + \beta^2 (R^2 + \delta^2)}$$

which can be rewritten as

$$r(1 - M_r) = \sqrt{\beta^2 R^2 + R^2 M_t^2 \cos^2 \gamma - 2RM_t \delta M_n \cos \gamma + \beta^2 \delta^2}$$

where

$$\beta_t^2 = 1 - M_t^2$$

Changing to Cartesian coordinates, since $R^2 = y_1^2 + y_2^2$ and $R \cos \gamma = y_2$, gives

$$r(1 - M_r) = \sqrt{\beta_y^2 y_1^2 + \beta_n^2 y_2^2 - 2M_t M_n \delta y_2 + \beta_t^2 \delta^2} \quad (16)$$

where

$$\beta_n^2 = 1 - M_n^2$$

This is now in a form that allows the integration of equation (12). It remains to write $M_r - M^2$ in terms of y_1 and y_2 ; from equation (15),

$$M_r - M^2 = \frac{\delta M_n - y_2 M_t}{r} \quad (17)$$

Substituting equations (16) and (17) in equation (12) gives

$$\begin{aligned} 4\pi p(\vec{x}_o, t) &= \int_{f=0} K_R dS + \int_{f=0} K_S dS \\ &+ M_n (\rho_o c^2 + p) \lim_{\delta \rightarrow 0} \int_{-\epsilon}^{\epsilon} \int_{-\epsilon}^{\epsilon} \frac{(\delta M_n - M_t y_2) dy_1 dy_2}{(\beta_y^2 y_1^2 + \beta_n^2 y_2^2 - 2\delta M_n M_t y_2 + \beta_t^2 \delta^2)^{3/2}} \\ &+ \beta_t^2 p \lim_{\delta \rightarrow 0} \int_{-\epsilon}^{\epsilon} \int_{-\epsilon}^{\epsilon} \frac{\delta dy_1 dy_2}{(\beta_y^2 y_1^2 + \beta_n^2 y_2^2 - 2\delta M_n M_t y_2 + \beta_t^2 \delta^2)^{3/2}} + O(\epsilon) \end{aligned}$$

which can be simplified to

$$\begin{aligned} 4\pi p(\vec{x}_o, t) &= \int_{f=0} K_R dS + \int_{f=0} K_S dS \\ &+ (\rho_o v_n^2 + \beta_t^2 p) \lim_{\delta \rightarrow 0} \int_{-\epsilon}^{\epsilon} \int_{-\epsilon}^{\epsilon} \frac{\delta dy_1 dy_2}{(\beta_y^2 y_1^2 + \beta_n^2 y_2^2 - 2\delta M_n M_t y_2 + \beta_t^2 \delta^2)^{3/2}} \\ &- M_n M_t (\rho_o c^2 + p) \lim_{\delta \rightarrow 0} \int_{-\epsilon}^{\epsilon} \int_{-\epsilon}^{\epsilon} \frac{y_2 dy_1 dy_2}{(\beta_y^2 y_1^2 + \beta_n^2 y_2^2 - 2\delta M_n M_t y_2 + \beta_t^2 \delta^2)^{3/2}} + O(\epsilon) \end{aligned}$$

Now, to integrate these the following transformations are used:

$$\eta = \beta_n^2 y_2 - M_n M_t \delta$$

$$\xi = \beta \beta_n y_1$$

Because the integrands are symmetric in y_1 , one gets

$$\begin{aligned} 4\pi p(\vec{x}_o, t) &= \int_{f=0} K_R dS + \int_{f=0} K_S dS \\ &+ (\rho_o v_n^2 + p) \lim_{\delta \rightarrow 0} \frac{2\beta}{\beta_n^2} \int_0^{\xi_2} \int_{\eta_1}^{\eta_2} \frac{\delta d\eta d\xi}{(\eta^2 + \xi^2 + \beta^2 \delta^2)^{3/2}} \\ &- M_n M_t (\rho_o c^2 + p) \lim_{\delta \rightarrow 0} \frac{2}{\beta \beta_n^2} \int_0^{\xi_2} \int_{\eta_1}^{\eta_2} \frac{\eta d\eta d\xi}{(\eta^2 + \xi^2 + \beta^2 \delta^2)^{3/2}} + O(\epsilon) \end{aligned}$$

where

$$\eta_1 = -\beta_n^2 \epsilon - M_n M_t \delta$$

$$\eta_2 = \beta_n^2 \epsilon - M_n M_t \delta$$

$$\xi_2 = \beta \beta_n \epsilon$$

Integrating these in the η -direction gives (ref. 52, p. 86)

$$\begin{aligned} 4\pi p(\vec{x}_o, t) &= \int_{f=0} K_R dS + \int_{f=0} K_S dS + \frac{2\beta}{\beta_n^2} (\rho_o v_n^2 + p) \\ &\times \lim_{\delta \rightarrow 0} \left[\int_0^{\xi_2} \frac{\delta \eta_2 d\xi}{(\xi^2 + \beta^2 \delta^2) \sqrt{\eta_2^2 + \xi^2 + \beta^2 \delta^2}} \right. \\ &\left. - \int_0^{\xi_2} \frac{\delta \eta_1 d\xi}{(\xi^2 + \beta^2 \delta^2) \sqrt{\eta_1^2 + \xi^2 + \beta^2 \delta^2}} \right] + \frac{2M_n M_t}{\beta \beta_n^2} (\rho_o c^2 + p) \\ &\times \lim_{\delta \rightarrow 0} \left(\int_0^{\xi_2} \frac{d\xi}{\sqrt{\eta_2^2 + \xi^2 + \beta^2 \delta^2}} - \int_0^{\xi_2} \frac{d\xi}{\sqrt{\eta_1^2 + \xi^2 + \beta^2 \delta^2}} \right) + O(\epsilon) \end{aligned}$$

Integrating these in the ξ -direction gives (ref. 52, pp. 60 and 89)

$$\begin{aligned}
4\pi p(\vec{x}_O, t) &= \int_{f=0} K_R dS + \int_{f=0} K_S dS + \frac{2}{\beta_n^2}(\rho_O v_n^2 + p) \\
&\times \lim_{\delta \rightarrow 0} \left[\frac{\delta \eta_2}{|\delta \eta_2|} \tan^{-1} \left(\left| \frac{\eta_2}{\delta} \right| \frac{\beta_n \epsilon}{\sqrt{\eta_2^2 + \beta_n^2 \beta_n^2 \epsilon^2 + \beta_n^2 \delta^2}} \right) - \frac{\delta \eta_1}{|\delta \eta_1|} \right. \\
&\times \left. \tan^{-1} \left(\left| \frac{\eta_1}{\delta} \right| \frac{\beta_n \epsilon}{\sqrt{\eta_1^2 + \beta_n^2 \beta_n^2 \epsilon^2 + \beta_n^2 \delta^2}} \right) \right] + \frac{2M}{\beta_n^2} \frac{M}{n t} (\rho_O c^2 + p) \\
&\times \lim_{\delta \rightarrow 0} \left[\ln \left(\frac{\sqrt{\eta_2^2 + \beta_n^2 \beta_n^2 \epsilon^2 + \beta_n^2 \delta^2} + \beta_n \epsilon}{\sqrt{\eta_1^2 + \beta_n^2 \beta_n^2 \epsilon^2 + \beta_n^2 \delta^2} + \beta_n \epsilon} \right) - \ln \left(\frac{\sqrt{\eta_2^2 + \beta_n^2 \delta^2}}{\sqrt{\eta_1^2 + \beta_n^2 \delta^2}} \right) \right] + O(\epsilon) \quad (18)
\end{aligned}$$

where the following transformation is used:

$$\xi' = \frac{\xi}{\sqrt{\eta_{1,2}^2 + \xi^2 + \beta_n^2 \delta^2}}$$

where $\eta_{1,2}^2$ signifies η_1 or η_2 , whichever is appropriate. Also it is assumed

that $M < 1$, so that $\beta > 0$. Notice that when $c \rightarrow \infty$, equation (18) reduces to the equation of Bisplinghoff et al. (ref. 44, p. 212) for incompressible flow.

Now since

$$\lim_{\delta \rightarrow 0} \eta_2 = -\lim_{\delta \rightarrow 0} \eta_1 = \beta_n^2 \epsilon$$

the logarithmic terms both become zero. Also the inverse tangent terms are equal in the limit as $\delta \rightarrow 0$ and behave like

$$\tan^{-1} \left(\left| \frac{\beta_n^2 \epsilon}{\delta} \right| \frac{\beta_n \epsilon}{\sqrt{\beta_n^4 \epsilon^2 + \beta_n^2 \beta_n^2 \epsilon^2 + \beta_n^2 \delta^2}} \right)$$

which is $\pi/2$ in the limit. Thus equation (18) becomes

$$4\pi p(\vec{x}_O, t) = \int_{f=0} K_R dS + \int_{f=0} K_S dS + \frac{2\pi \operatorname{sgn}(\delta)}{\beta_n^2} (\rho_O v_n^2 + p) + O(\epsilon) \quad (19)$$

which reduces to

$$4\pi \left(1 - \frac{1}{2\beta_n^2} \right) p(\vec{x}_O, t) = \int_{f=0} K_R dS + \int_{f=0} K_S dS + \frac{2\pi \rho_O v_n^2(\vec{x}_O, t)}{\beta_n^2} + O(\epsilon) \quad (20)$$

where the integrands are repeated for convenience:

$$K_R = \left\{ \frac{\rho_o c^2 M_n \dot{M}_r + p \Omega_r (1 - M_r) + p \dot{M}_r \cos \theta}{cr(1 - M_r)^3} \right\}_{ret}$$

$$K_S = \left\{ \frac{\rho_o c^2 M_n (M_r - M^2) + p[(1 - M^2) \cos \theta - (1 - M_r) M_n]}{r^2 (1 - M_r)^3} \right\}_{ret}$$

Equation (20) represents the governing equation, amenable now to numerical techniques, for the pressure on a body in compressible subsonic motion. The theory is linearized so that it is expected to be more and more accurate for thin or slender bodies, including most bodies of aerodynamic interest. For completeness, note that for the observer inside the body, $\text{sgn}(\delta) = -1$; and outside of the body, $\text{sgn}(\delta) = 1$. Thus, equation (20) applies to the outside of the body.

As mentioned in the Introduction (section I.A), these results do not agree with those of Morino (ref. 17, appendix C), although a direct comparison is difficult since he uses a velocity-potential formulation. Nevertheless, a few discrepancies between the results can be noted. In this section we have calculated the contribution from a square ϵ -region. These results are shown to be Mach number dependent since the coefficients in equation (20) include β_n . Morino claims that the contribution from the ϵ -region is independent of Mach number, simply 2π , which is the incompressible result. In addition, his ϵ -region is circular. Since the ϵ -regions are analogous to the panels in a panel method, it is difficult to understand how one can model a body using circular panels. Furthermore, Farassat (ref. 7) has calculated the contribution from a circular ϵ -region for the FW-H equation, and the result differs from the result in this section and also from the results of Morino. Thus one cannot assume that differently shaped ϵ -regions yield the same result. However, the results presented here can be shown to be unchanged for any quadrilateral that is symmetric about y_2 , even if one side has zero length.

D. Reduction to Incompressible Aerodynamics

Since equation (20), especially the integrands K_R and K_S , is relatively complicated, it is useful to reduce it to its incompressible form. If the limit is taken as $c \rightarrow \infty$, all the Mach number terms (M_n , M_r , M , and \dot{M}_r) approach zero. Furthermore, all the β terms (β , β_t , and β_n) approach unity. Thus, $K_R = 0$ and

$$K_S = \frac{\rho_o v_n v_r + p \cos \theta}{r^2}$$

Therefore, equation (20) becomes in the incompressible limit

$$2\pi p(\vec{x}_o) = \int_{f=0} \frac{\rho_o v_n v_r + p \cos \theta}{r^2} dS + 2\pi \rho_o v_n^2$$

This could have been obtained by taking the limit as $c \rightarrow \infty$ of the FW-H equation and then solving it using the Green's function of potential theory.

The first term in the integrand is due to the thickness term of the FW-H equation. It is also equivalent to the thickness term of incompressible aerodynamics, equation (5-85) of reference 44.

The second term in the integrand is called the "loading" term in aeroacoustics. It is directly related to the lifting effects in aerodynamics, for example, equation (5-94) of reference 44.

Throughout this study it has always been useful to refer to the above equation for guidance. The reader is encouraged to do so also when something related to the full equation is unclear. Of course retarded time effects are not included in the above equation because of the infinite speed of sound propagation.

III. COMPUTATIONAL METHOD

A. Approximating Body by a Finite Number of Panels

The complexity of equation (20) precludes an analytic solution for most, if not all, bodies of interest. Therefore one must use approximate numerical methods. The analysis in the previous section showed that the solution can be approximated to $O(\epsilon)$ where ϵ^2 is the area of a hole removed from the region of integration. This procedure was shown to be analogous to taking the Cauchy principal value which is also an approximation that is accurate to the order of the size of the hole deleted from the integration.

In the past, to predict the noise due to bodies in motion, one needed the surface pressure. Now, using equation (20), one can calculate the pressure on a small region of the body, given the pressure on the remainder of the body. By discretizing the surface, one can develop a system of algebraic equations whose solution gives the pressure everywhere on the body. To do this, the body must be approximated by a finite number of planar elements, or panels. The pressure is assumed constant over each element. The solution approaches the exact solution as $\epsilon \rightarrow 0$.

As mentioned earlier, the ϵ -region corresponds to a small area of the surface immediately around the observer. To develop the system of algebraic equations, the observer must be located on each panel of the body successively. Each location of the observer yields an algebraic equation.

Recognizing the above, one can proceed in several ways to solve the equation numerically. They differ in how the dependent variable is assumed to behave. One method that has been used on similar equations is a collocation procedure (ref. 53) using global shape or loading functions. This method is common in lifting surface theory (refs. 54 and 55), where the loading functions are chosen to exactly satisfy the leading-edge, trailing-edge, and tip conditions and to produce satisfactory numerical results. Once these functions are selected, there are still integrations to perform, although these are now over known functions and may permit analytic evaluation. Otherwise quadrature is necessary.

The collocation method was not selected for the present work because of its lack of generality: the shape functions required depend on the body shape. For example,

one may have to use a different set of functions for a fuselage, a propeller, and a wing - not to mention for more complicated shapes such as highly swept propeller blades.

Since the purpose of the numerical procedure in the present work was to verify the feasibility of the method and not to develop a production computer program, it seemed appropriate to solve the equation directly rather than to introduce additional complications. Therefore, the computer program that was developed uses only quadrature. The dependent variable is not represented by global shape functions. Of course, more efficient or sophisticated methods may be available for particular applications. As an initial solution method however, this approach brought out the subtleties and pitfalls of the equation better than any other. A disadvantage of the method is that it produces a large system of equations, but they are strongly diagonal. Therefore the system of equations is readily solved.

Quadrature is used over each element. As mentioned earlier, the observer, at \vec{x}_o , is positioned on each element successively (at time t). The observer is stationary, so one must specify the time on the body. For the observer on a given panel, the numerical integrations are carried out over all the other panels. The theoretical developments presented earlier have already calculated the effect that the observer panel has on itself.

For a body approximated by N panels as in figure 3, the approximate form of equation (20) is

$$4\pi \left(1 - \frac{1}{2\beta_n^2}\right) p_i - \sum_{\substack{j=1 \\ j \neq i}}^N p_j \iint_{j} K_p dS = \frac{2\pi\rho_o v_{ni}^2}{\beta_n^2} + \sum_{\substack{j=1 \\ j \neq i}}^N \iint_{j} K_v dS \quad (21)$$

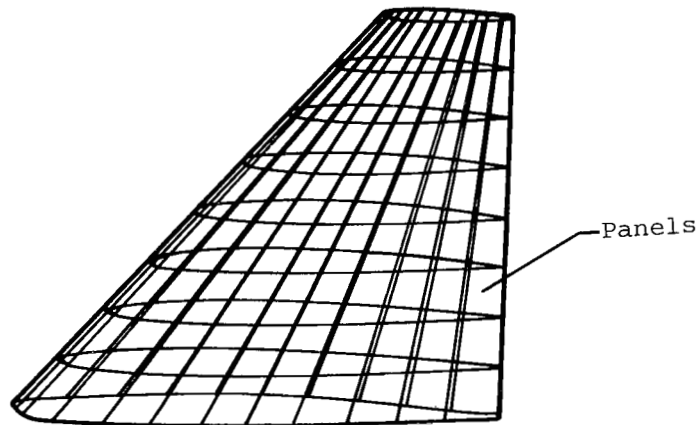


Figure 3.- Body approximated by panels.

where

$$K_p = \left[\frac{\Omega_r (1 - M_r) + \dot{M}_r \cos \theta}{cr(1 - M_r)^3} + \frac{(1 - M^2) \cos \theta - (1 - M_r)M_n}{r^2(1 - M_r)^3} \right]_{ret}$$

$$K_v = \rho_o c^2 \left[\frac{M_n \dot{M}_r}{cr(1 - M_r)^3} + \frac{M_n (M_r - M^2)}{r^2 (1 - M_r)^3} \right]_{ret}$$

and subscripts i and j signify the observer and source panels, respectively; the observer and source are assumed to be at the centroid of the respective panels. Equation (21) is one equation for N unknowns, p_i and p_j ($j = 1, \dots, N$, $j \neq i$). Letting i take on the values from 1 to N gives a system of N equations for N unknowns.

This system of equations can be expressed by a matrix multiplying a vector of unknowns equal to another vector: The coefficients of p_i are the diagonal terms of the matrix. The integrals over K_p are the off-diagonal terms. The right hand side of equation (21) yields a unique value for index i .

B. Quadrature Formulas

Legendre-Gauss quadrature formulas are used to calculate the integrals

$$\iint_j K_p dS \quad \text{and} \quad \iint_j K_v dS$$

Portions of each integral can be ill-behaved because of the $1/r^2$ terms in it. Even though the effect an element has on itself has been calculated, two different elements may be very close together, for example, on the upper and lower surfaces of a thin airfoil, especially at the trailing edge. One-dimensional Legendre-Gauss quadrature is exact for polynomials of order $(2n - 1)$ where n is the number of nodes. For the above integrals this may not be sufficient. They may require very high order polynomials to approximate their behavior because of the negative exponent on r .

Just as for the analytical part of this work, the numerical solution would be trivial if not for the ill-behaved nature of the integrands. Since this does represent the most difficult aspect of the computational method, two simple examples are given to illustrate the singular behavior of the integrals.

The ill-behaved terms in both K_p and K_v become simply $\cos \theta / r^2$ for incompressible flow. Thus the integrals become proportional to

$$I = \iint \frac{\cos \theta dS}{r^2}$$

Now for these examples, assume that the integration region (source panel) is a unit square and the observer is located along the normal directly above the center of the panel, as in figure 4. This is approximately the orientation of the two panels that lie directly across from one another on the upper and lower surfaces of an airfoil. The observer is at \vec{x} and the source point is at \vec{y} . Therefore, I represents the effect that the unit square has on the observer.

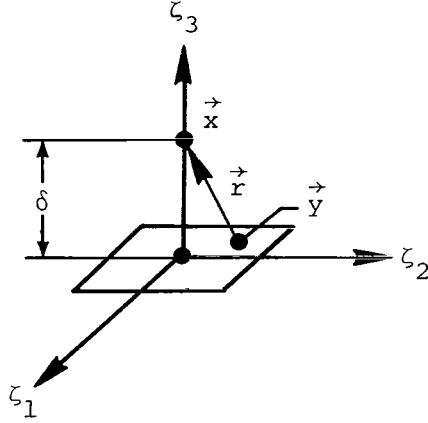


Figure 4.- Geometry near singularity in incompressible flow.

Note that

$$\frac{\cos \theta}{r^2} = \frac{\delta}{(\zeta_1^2 + \zeta_2^2 + \delta^2)^{3/2}}$$

and the integral becomes

$$I(\delta) = \int_{-1}^1 \int_{-1}^1 \frac{\delta \, d\zeta_1 \, d\zeta_2}{(\zeta_1^2 + \zeta_2^2 + \delta^2)^{3/2}} \quad (22)$$

which can be evaluated exactly as

$$I(\delta) = 4 \tan^{-1} \left(\frac{1}{\delta \sqrt{2 + \delta^2}} \right) \quad (23)$$

This integral illustrates the difficulty in solving equation (21) using quadrature. Notice that the integration is through the point $\zeta_1 = \zeta_2 = 0$, at which the integrand behaves like $1/\delta^2$. For small δ , it is very difficult to approximate with a polynomial a function that grows this rapidly. Were it not for this behavior for two panels close together, equation (21) would be relatively easy to solve. Also, because bodies of aerodynamic interest are usually thin, panels do lie close together.

Two approximations of the integral $I(\delta)$ using Legendre-Gauss quadrature (ref. 56) and different numbers of nodes are now presented. The one-dimensional formulas over a surface give

$$I(\delta) = \sum_{i=1}^{n'} \sum_{j=1}^{n'} \frac{H_i H_j \delta}{(\zeta_{1,i}^2 + \zeta_{2,j}^2 + \delta^2)^{3/2}}$$

where n' is the number of nodes in each direction, H_i and H_j are weight coefficients, and $(\zeta_{1,i}, \zeta_{2,j})$ are the node locations (given). The node locations and weight coefficients are given in appendix A. When $n' = 2$, the above formula simply becomes

$$I(\delta) = \frac{4\delta}{[2(0.57735)^2 + \delta^2]^{3/2}} \tag{24}$$

where all the weight coefficients are unity and all the nodes are at ± 0.577350 .

The important question is how accurately equation (24) models the exact solution, equation (23), for the various values of δ . One would expect it to be inaccurate for very small δ because the integrand varies so rapidly.

Figure 5 is a graph comparing the exact value of the integral $I(\delta)$ and numerical approximations to it. The abscissa uses the relation $1/\delta^2$ because this is proportional to

$$\text{Ratio} = \left[\frac{\cos \theta}{r^2 (1 - M_r)^3} \right]_{\text{ret}} dS$$

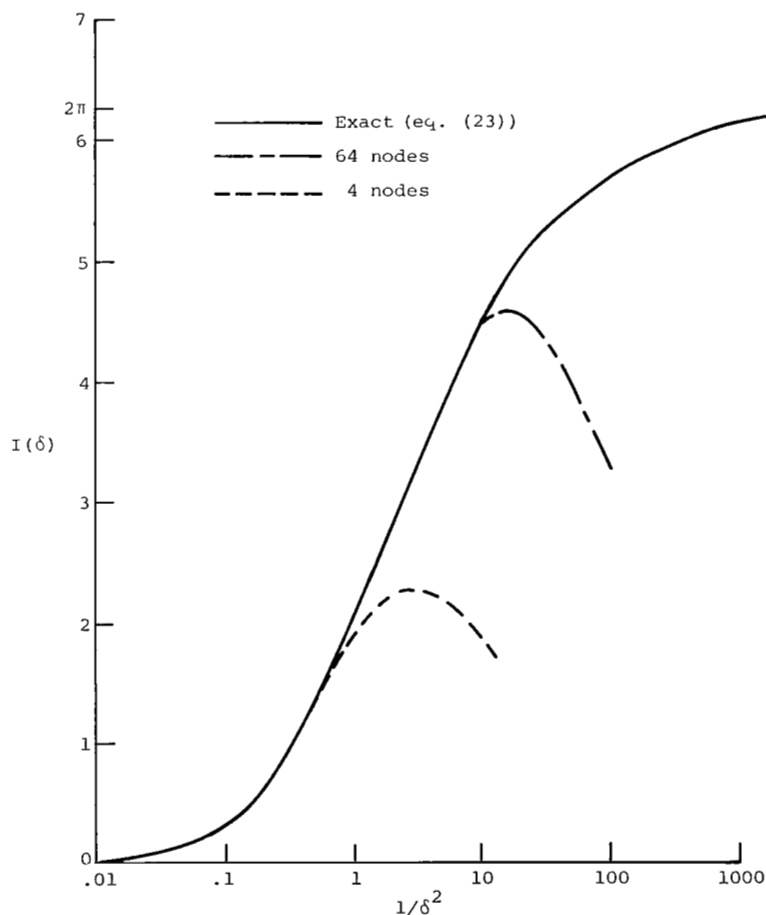


Figure 5.- Comparison of Legendre-Gauss quadrature and exact integration for sample integral.

which is used in the computer program to determine how many quadrature points to use. In addition to equations (23) and (24), the results from the use of an 8-point (64 points over a surface) quadrature formula are presented. For values of $1/\delta^2 < 0.19$, the 2-point formulas are accurate to at least 1 percent. This same degree of accuracy can be obtained for even larger values of $1/\delta^2$ using the 8-point formula. These approximate results diverge very rapidly from the exact value for δ near zero.

These comparisons not only illustrate the behavior of the integrals but also provide a means to determine what order quadrature should be used (i.e., how many nodes), given the area of a panel and the distance between the panel and the observer. To achieve reasonable efficiency and accuracy, several orders of quadrature formulas are used in the current computer program, which actually determines how many nodes to use for each integration. The maximum is 64 nodes over a panel. The minimum, for panels and observers far apart, is a simple 1-point rectangular rule. Further studies were conducted using quadrature formulas that were exact for trigonometric functions, but they offered no significant improvement in accuracy or efficiency.

In the computer program, for panels that have $\text{Ratio} > 16$, an exact form of the solution is used (eq. (18)), that is, the form of the equation before the limit as $\delta \rightarrow 0$ was taken. But because the observer is assumed (in the development of eq. (18)) to lie along the normal to the source panel, this formula can be used only for panels oriented in this manner. This does not represent a problem though, since the panels on an aerodynamic body that are closest together (e.g., at the trailing edge) are so oriented.

C. Jacobians and Mapping of Elements

Since Legendre-Gauss quadrature requires the integration region to extend from -1 to 1, each element must be mapped to a unit square, by using standard finite-element transformations. Of course, to integrate over the mapped element, one must also calculate the Jacobian of the transformation. This section briefly describes the methods used to perform these operations.

The elements that make up the bodies are all in three-dimensional space. They are in motion, but that does not enter into the following considerations. The retarded time aspects affect only the integrands and not the integration surface directly.

The required integrals are of the form

$$I = \iint_{\text{Panel}} K(x, y, z) \, dS$$

To reduce confusion, the Cartesian coordinate system is denoted by x , y , and z rather than by x_1 , x_2 , and x_3 . If this panel is mapped to the $\eta_3 = 0$ plane of the $\vec{\eta}$ -frame, it becomes (ref. 57)

$$I = \int_{-1}^1 \int_{-1}^1 K[x(\eta_1, \eta_2), y(\eta_1, \eta_2), z(\eta_1, \eta_2)] |J| \, d\eta_1 \, d\eta_2$$

where

$$|J| = \begin{vmatrix} \hat{i} & \hat{j} & \hat{k} \\ \frac{\partial x}{\partial \eta_1} & \frac{\partial y}{\partial \eta_1} & \frac{\partial z}{\partial \eta_1} \\ \frac{\partial x}{\partial \eta_2} & \frac{\partial y}{\partial \eta_2} & \frac{\partial z}{\partial \eta_2} \end{vmatrix} \quad (25)$$

The panels are mapped to the $\vec{\eta}$ -frame with linear finite element shape functions (ref. 58) of the form,

$$\left. \begin{aligned} x(\eta_1, \eta_2) &= \sum_{i=1}^4 f_i x_i \\ y(\eta_1, \eta_2) &= \sum_{i=1}^4 f_i y_i \\ z(\eta_1, \eta_2) &= \sum_{i=1}^4 f_i z_i \end{aligned} \right\} \quad (26)$$

where x_i , y_i , and z_i ($i = 1$ to 4) represent the vector components of the corners of the source panels in the original coordinate system. Further,

$$\begin{bmatrix} f_1 \\ f_2 \\ f_3 \\ f_4 \end{bmatrix} = \frac{1}{4} \begin{bmatrix} (1 - \eta_1)(1 - \eta_2) \\ (1 - \eta_1)(1 + \eta_2) \\ (1 + \eta_1)(1 + \eta_2) \\ (1 + \eta_1)(1 - \eta_2) \end{bmatrix}$$

The Jacobian at any particular value of η_1 and η_2 is obtained by differentiating the above formulas and using equation (25). For example,

$$\frac{\partial x}{\partial \eta_1} = \frac{-1}{4} [(1 - \eta_2)x_1 + (1 + \eta_2)x_2 - (1 + \eta_2)x_3 - (1 - \eta_2)x_4]$$

These formulas are used in the subroutines JACOBI and NODE. A flowchart of all the subroutines in the computer program is given in appendix B. In JACOBI, the Jacobian at every node on every element is calculated and stored. Since it is not known a priori how many nodes are required to perform the integrations, the Jacobians for

each element are calculated for 1-, 4-, 16-, and 64-node quadrature. Thus, the Jacobian is calculated for 85 points on each panel. All these Jacobians are stored except the 64-node values, which are calculated when needed. This means that $21N$ Jacobians are stored, where N is the number of elements.

Given a node η_1 and η_2 , subroutine NODE calculates x , y , and z from equations (26). Values of η_1 and η_2 corresponding to Legendre-Gauss quadrature (see appendix A) are stored in DATA statements at the beginning of the main program.

It is important to point out that the Jacobians must be calculated only once for a given body. Changes in angle of attack or velocity do not affect them.

D. Retarded Time Calculation

Retarded time is another quantity that must be calculated numerically. It is typically governed by a transcendental equation that is difficult to solve analytically. In this section, the governing equation is derived for retarded time for a body that is moving rectilinearly (along the z -axis) and spinning (about the z -axis) (see fig. 6). This motion is not the most general type possible but is adequate to test the theory for several types of bodies. For instance, because the spinning is about the same axis as the rectilinear motion, the motion of a helicopter blade in forward flight could not be represented with the governing equation derived here. However, other types of motions should be relatively easy to include in future programs.

The quantity to be calculated is r_{ret} , the retarded time distance between an observer and a source point. This is the r that appears throughout this study, for example, in equation (8). It represents the propagation distance for a signal emitted from a source that is in motion. The observer is stationary, as has been assumed throughout the report.

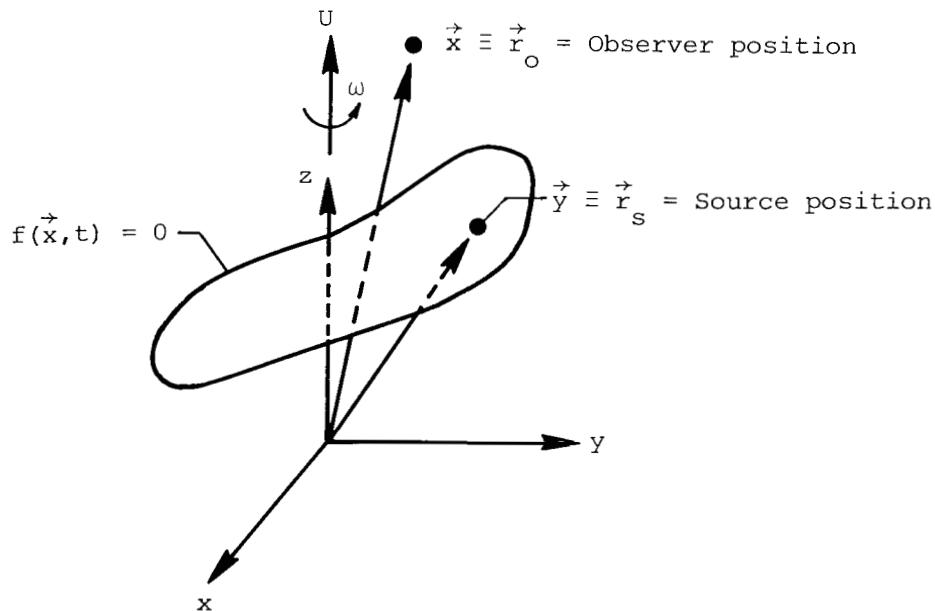


Figure 6.- Velocities and position vectors used in retarded time calculations.

In Cartesian coordinates, the observer is located at

$$\vec{r}_o = [x_o, y_o, z_o]$$

and the source in motion is located at

$$\vec{r}_s(\tau) = [x_s \cos(\omega\tau) - y_s \sin(\omega\tau), x_s \sin(\omega\tau) + y_s \cos(\omega\tau), z_s + U\tau]$$

where $\tau = t - r/c$, ω is the angular velocity of the body, and U is the rectilinear velocity of the body. When $\tau = 0$, the source is at $[x_s, y_s, z_s]$.

Now from its definition,

$$\vec{r}_{ret} = [\vec{r}_o - \vec{r}_s(\tau)]_{ret} = \vec{r}_o - \vec{r}_s\left(t - \frac{r}{c}\right)$$

Therefore,

$$r^2 = |\vec{r}|^2 = \{r_o^2 + r_s^2 - 2R_s [x_o \cos(\omega\tau) + y_o \sin(\omega\tau)] + 2U\tau(z_s - z_o) + U^2\tau^2 - 2z_o z_s\}_{ret}$$

where

$$r_o^2 = x_o^2 + y_o^2 + z_o^2$$

$$r_s^2 \equiv x_s^2 + y_s^2 + z_s^2$$

$$R_s^2 \equiv x_s^2 + y_s^2$$

Since only steady motion is being considered, the choice of a particular value of t is arbitrary. The pressure is not changing with time (in these body-fixed coordinates). Therefore, setting $t = 0$ gives

$$(1 - M^2)r^2 + 2M(z_s - z_o)r - \left[r_o^2 + r_s^2 - 2(x_o x_s + y_o y_s) \cos\left(\frac{\omega r}{c}\right) + 2(y_o x_s - x_o y_s) \sin\left(\frac{\omega r}{c}\right) - 2z_o z_s \right] = 0$$

This is the transcendental equation governing r_{ret} . In subroutine RADIUS (see appendix B) this equation is solved with a Newton-Raphson technique (ref. 56).

Once r_{ret} is determined, it can be used to calculate the vector quantity \vec{r}_{ret} from

$$\vec{r}_{ret} = \left[x_o - x_s \cos\left(\frac{\omega r}{c}\right) - y_s \sin\left(\frac{\omega r}{c}\right), y_o + x_s \sin\left(\frac{\omega r}{c}\right) - y_s \cos\left(\frac{\omega r}{c}\right), z_o - z_s + \frac{Ur}{c} \right]$$

E. Computer Program

This section describes the complete computer program. The major tasks of the program are described in the order in which they are performed, as shown in the flowchart in figures 7 and 8.

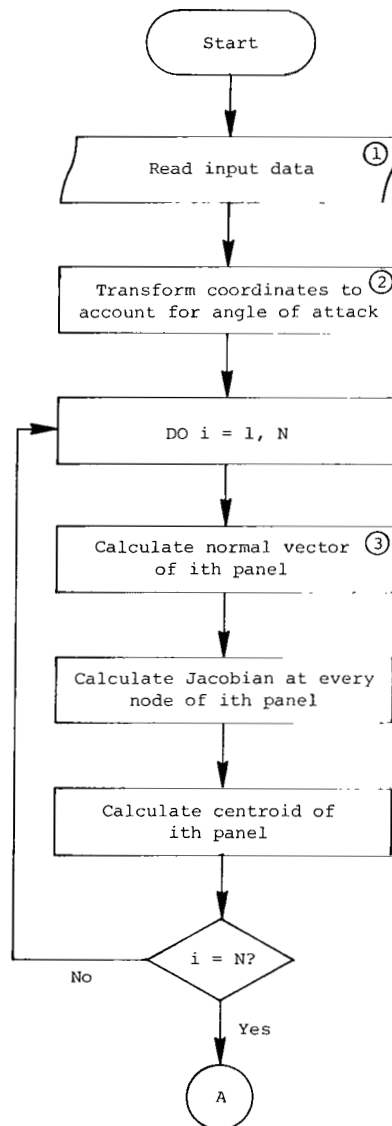


Figure 7.- Computer program flowchart, part I.

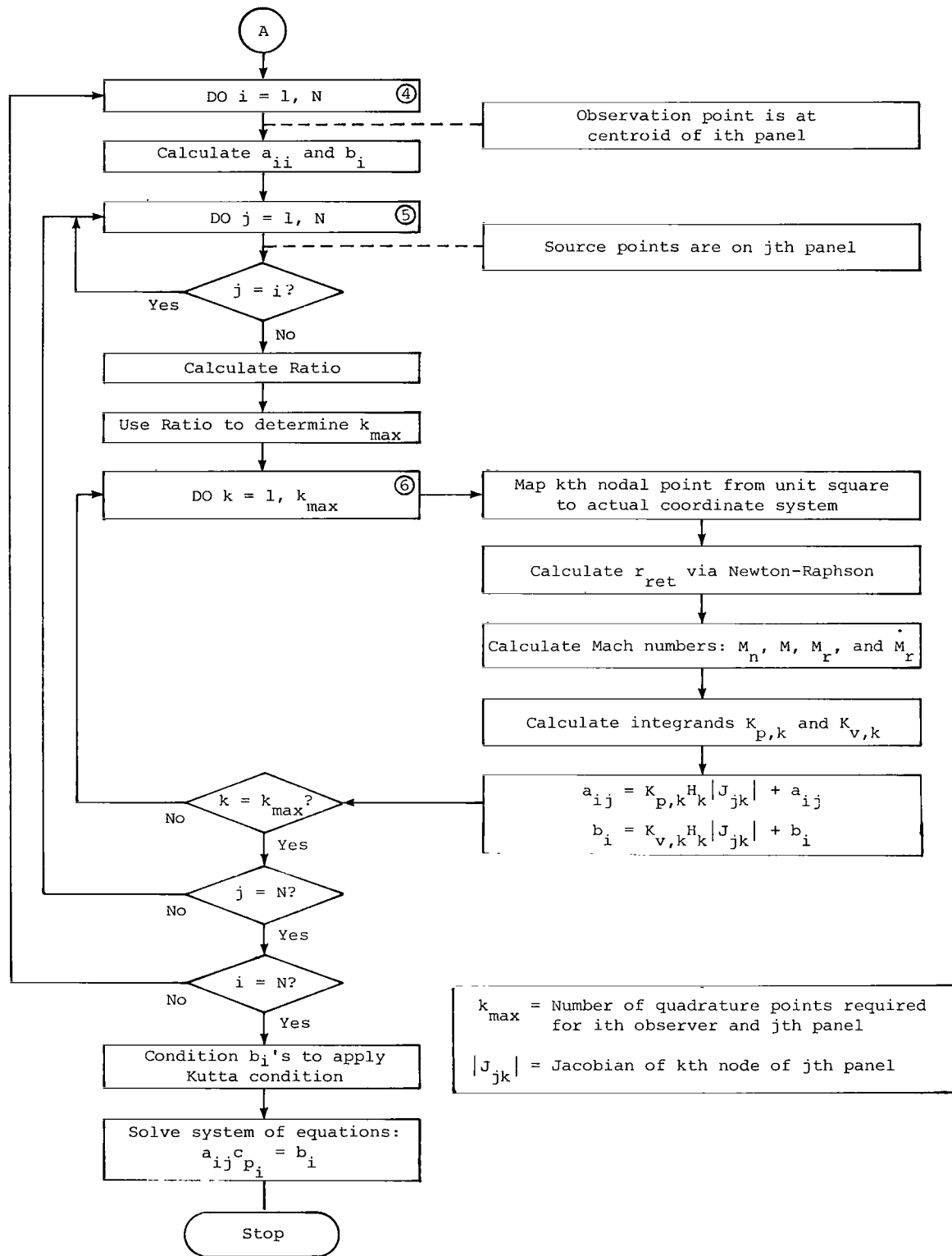


Figure 8.- Computer program flowchart, part II.

The first major task of the program is to read an input file that describes the body and its velocity (box 1). The body is described by a finite number of coordinate points in three-dimensional space. These must be input properly to form the elements. They are input in the order shown in figure 9, which shows a wedge-shaped airfoil. The corresponding element numbers are shown in figure 10. Each cross section must have the same number of points, although this would not have to be so in future programs. Note that to "close" each cross section, the first and last

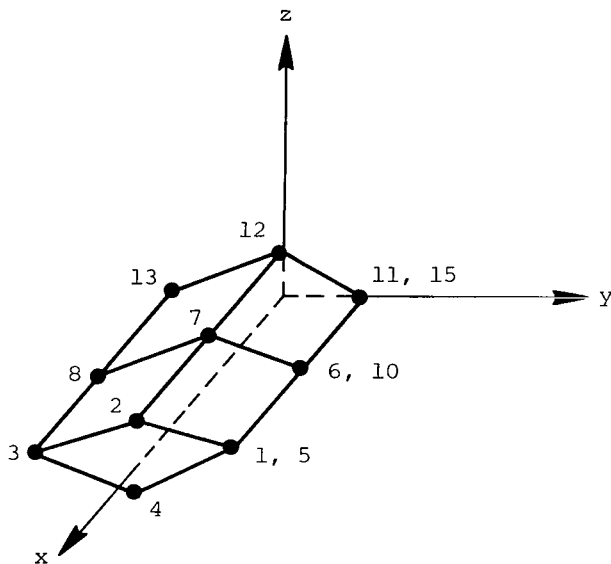


Figure 9.- Proper order of input coordinate points.

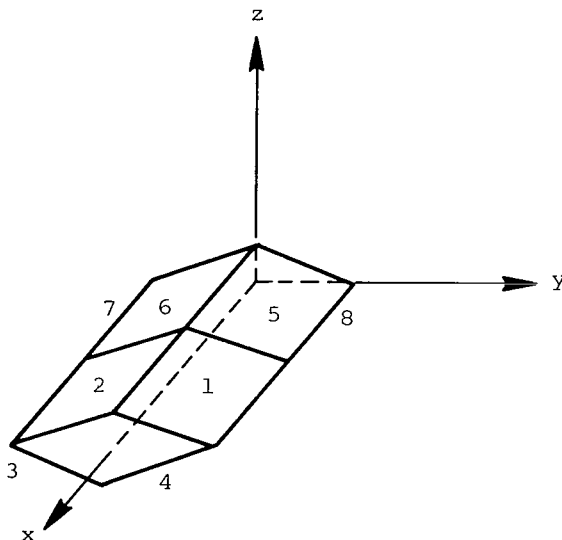


Figure 10.- Numbering of elements.

coordinate points are coincident. A good way to check the input points is to examine the normal vectors that the program calculates. Quite often if the points are input in an improper manner, the normals point into the body.

The next step in the code is to transform the coordinates to account for the angle of attack (box 2). This could also be used to change a set of coordinates describing a rotating blade to those describing a wing in rectilinear motion ($\alpha = 90^\circ$). Since rectilinear motion is always in the direction of the z-axis and spinning occurs about this axis, the body would have to be rotated to switch roles from a blade to a wing.

The current program is designed to run only one angle of attack at a time. Ideally, for a production code, another loop would be added to calculate multiple right hand sides (RHS) of equation (21). Remember it is necessary to calculate the left hand side only once for a given Mach number, but the RHS varies for each angle of attack. This procedure would be especially efficient since most linear equation solvers are equipped to handle multiple RHS and give multiple solutions. The matrix would be manipulated only once.

The next major section of the program (box 3, fig. 7) is a loop that calculates normal vectors, Jacobians, and centroids of each element. The normal vectors are calculated in the main program using a technique described by Hess (ref. 27), which simply takes the vector cross product of the diagonals of each panel.

Jacobians are calculated in the subroutine called JACOBI (see appendix B) using the formulas presented in section III.C. The centroids are calculated in subroutine CENTER by integrating over each panel. Since the nodes and Jacobians are already calculated and stored, this is relatively straightforward. The area of any panel can be calculated simply by adding the four Jacobians calculated for the two-point Legendre-Gauss quadrature for that element, since the weight functions for the two-point formulas are unity.

At this point in the program all the preliminaries have been completed. The remainder of the program is shown in figure 8, the second part of the flowchart. The first DO-loop, over i (box 4), places the observer on each element successively. For each location of the observer, all the other panels are successively treated as sources by the next DO-loop over j (box 5). Quadrature is performed over each source panel.

Before the quadrature is performed, the program must determine how many quadrature points to use. For each value of i and j , the quantity

$$\text{Ratio} = \left[\frac{\cos \theta}{r^2 (1 - M_r)^3} \right]_{\text{ret}} dS$$

is calculated, where \vec{x} and \vec{y} are taken as the centroids of the i and j panels, respectively. As shown earlier in section III.B, the number of nodes required for accurate quadrature is highly dependent on this quantity. Therefore, the program calculates this quantity in subroutine TEST and determines how many quadrature points to use. The area of the source panel is used for dS , of course.

Once the appropriate number of nodes to use is determined, the actual quadrature calculation begins at the DO-loop over k (box 6). The number of nodes it will use

for that particular integration is k_{\max} . Subroutine NODE determines from equation (26) the location of the node in body coordinates from the Gaussian nodal coordinates. Then subroutine RADIUS calculates the retarded time propagation distance \vec{r}_{ret} . Subroutine MACH calculates M , M_r , M_n , and \dot{M}_r . With these quantities calculated, the integrands K_p and K_v can be computed for equation (21). By multiplying the integrands, the weight coefficients, and the Jacobian at each node, and then adding these products from each node, the integration is complete over a particular panel.

After the DO-loop over i is completed, the system of algebraic equations is completely developed. The solution to the system of equations is obtained using subroutine INVERT, which, in addition, conditions the equations to satisfy a Kutta condition. This conditioning is described in the next section. The final step of solving these equations is performed using a NASA Langley Research Center library subroutine called GELIM (ref. 59), which uses an upper or lower decomposition as described in reference 56.

IV. LIFTING BODIES

Determining the surface pressure on lifting bodies is, of course, much more difficult than on nonlifting bodies because lift is an inherently viscous effect. To approximate viscous effects with an inviscid theory, one must obviously use not only physics but also experimental results to extend the theory. But, as Hess (ref. 26) states:

It is important to realize that any such formulation is simply a...model of real lifting flow, and that the two flows are not necessarily related in any fundamental way.

In this section the major differences between inviscid and viscous theory are briefly described, as they relate to aerodynamics. After that a method for using the present theory to approximate the effects due to viscosity is presented. These discussions are more qualitative than quantitative.

The linearized, inviscid equations used herein neglect several important features of the actual flow. First, the flow is assumed to slip over the body, which means that no tangential velocity boundary condition is prescribed. This immediately leads to a question of uniqueness, for there are an infinite number of velocity fields that satisfy the normal velocity boundary condition. The Kutta, or trailing edge, condition is usually used to determine which of these velocity fields is appropriate, since it is known that viscosity prevents the flow from turning the sharp angle at the trailing edge.

Neglecting the no-slip condition also means that there would be no boundary layer or wake in this inviscid flow, although there could be a layer of zero thickness over which a tangential velocity jump occurs. Since the pressure is continuous across such a layer, this jump does not affect the formulation when using the pressure as the dependent variable, as mentioned in section I.A.

A convenient, and computationally inexpensive, way to account for the boundary layer occurring in real flows is to use the displacement effect (refs. 35, 60, and 61) via an iterative technique. First, the inviscid calculations are performed with no boundary layer assumed. Then, from these results, the displacement thick-

ness is calculated. The boundary layer and its effect on the streamlines is then accounted for by enlarging the actual body by an amount equal to the displacement thickness.

Another difficulty in using the FW-H equation to predict lift is that there is no built-in mechanism to generate lift. The circulation is assumed to be zero. The well-known panel methods distribute line vortices on or inside the body, where their strengths are determined by satisfying a Kutta condition. These vortices simply provide a means of altering the onset flow by providing a circulatory contribution to the flow. Of course, one must still satisfy the normal velocity boundary condition. Using the FW-H equation as the governing equation means that there is no simple way to include line vortices. Fortunately, there is a way to condition the final system of linear equations and obtain the effects due to lift without using the concept of vortices distributed within the body.

To understand fully the technique used to condition the equations, one must consider what the flow field is really like around a lifting airfoil. A major difference between a lifting and a nonlifting airfoil is the location of the leading-edge stagnation point. Conversely, the Kutta condition tells us that the trailing-edge stagnation point is in the same location for lifting and nonlifting airfoils. Furthermore, even the streamlines near the trailing edge are remarkably similar for lifting and nonlifting airfoils. Thus, the trailing edge experiences essentially the same flow whether the body is at an angle of attack or not. Van Holten (ref. 12) essentially implies this fact when he advocates placing only the leading edge at an angle of attack. He uses the acceleration potential and finds that using this "variable-geometry" concept forces his inviscid results into close agreement with real lifting flows. Apparently, these ideas can be traced back to Lanchester.

To illustrate why Van Holten's suggestion works, several numerical examples are presented for a simple body made up of only six elements. By presenting numerical results for a simple body, the procedures should become clearer. Thus, equation (20) is solved numerically by the computer program described in the previous section for the body shown in figure 11, a crude six-element model of a wing with an aspect ratio of 3. The profile, which is roughly that of an NACA 0012 airfoil, is shown in figure 12. Using this simple body allows one to investigate the numerical procedure and to illustrate how the effects due to lift are included. The aspect ratio is deliberately kept small so that only a few elements need be used.

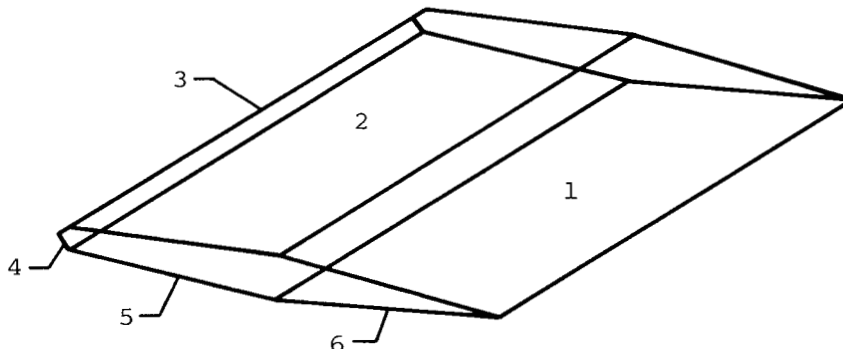


Figure 11.- Simple six-element airfoil with element numbers.



Figure 12.- Profile of simple six-element airfoil.

The first example is for the body in very low-speed rectilinear motion ($M = 0.03$) at an angle of attack of zero. The resulting system of equations is

$$\begin{bmatrix} 2\pi & 0.19 & 0.07 & 0.07 & 0.43 & 5.43 \\ 0.20 & 2\pi & .19 & .25 & 4.92 & .61 \\ .17 & .28 & 2\pi & .10 & .82 & .22 \\ .22 & .82 & .10 & 2\pi & .28 & .17 \\ .61 & 4.92 & .25 & .19 & 2\pi & .20 \\ 5.43 & .43 & .07 & .07 & .19 & 2\pi \end{bmatrix} \begin{bmatrix} c_{p_1} \\ c_{p_2} \\ c_{p_3} \\ c_{p_4} \\ c_{p_5} \\ c_{p_6} \end{bmatrix} = \begin{bmatrix} -0.66 \\ -1.70 \\ 6.17 \\ 6.17 \\ -1.70 \\ -.66 \end{bmatrix} \quad (27)$$

where c_{p_i} is the pressure coefficient on i th element. The solution to equations (27) is shown in figure 13. It differs markedly from the results for the two-dimensional airfoil (from ref. 62) which are also shown, but that is to be expected since the aspect ratio is only 3 and the paneling is very crude. However, it does show the proper trend, which is all that is desired since these discussions are designed only to illustrate the general behavior of the equations. An alternative approach of discussing these ideas using the equations themselves is possible but would probably not be as successful in instilling an intuitive feeling since the discussion would be very abstract. Much can be learned concerning equation (20) from the examples included herein.

Getting back to the example, notice that in equations (27), there is a symmetry defined by:

$$a_{ij} = a_{7-i,7-j}$$

$$b_i = b_{7-i}$$

where i and j range from 1 to 6. This means that the pressure on the upper and lower surfaces is governed by the same equation, since the airfoil is symmetric and

at zero angle of attack, so that the upper and lower surfaces experience the same flow. It also means that

$$c_{P_i} = c_{P_{7-i}}$$

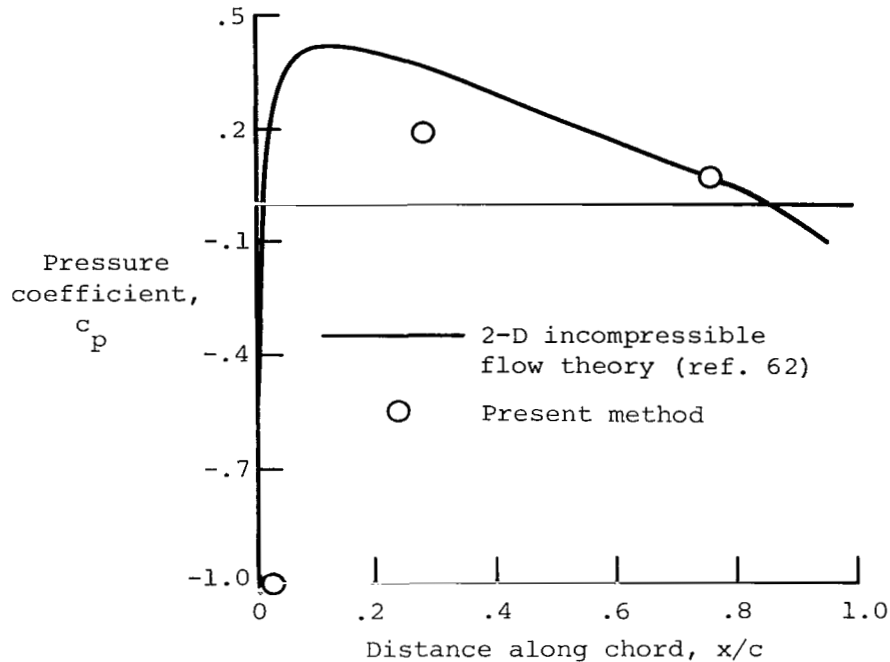


Figure 13.- Pressure distribution on simple six-element airfoil.

Another important point is that some of the off-diagonal terms in the matrix are nearly as large as the diagonal terms, especially for the panels at the trailing edge (the first and last rows of the matrix), because they are so close together. The effect one of these panels has on another is nearly the same as the effect one has on itself. In addition, these large off-diagonal terms are the most difficult to calculate, as discussed in section III.B. For an infinitely thin body, these large off-diagonal terms would be equal to the diagonal terms. Kuo and Morino (ref. 63) observed this fact also, but found that it did not cause any serious numerical problems for bodies of interest. It is also of interest to note that for an infinitely thin body the right-hand-side vector would be zero. Therefore, one would obtain the result

$$c_{P_{upper}} = -c_{P_{lower}}$$

and consequently zero lift.

The really interesting features appear when the body is placed at an angle of attack. Using the same airfoil as in the previous example but at an angle of 10° yields the following system of equations:

$$\begin{bmatrix} 2\pi & 0.19 & 0.07 & 0.07 & 0.43 & 5.43 \\ 0.20 & 2\pi & .19 & .25 & 4.92 & .61 \\ .17 & .28 & 2\pi & .10 & .82 & .22 \\ .22 & .82 & .10 & 2\pi & .28 & .17 \\ .61 & 4.92 & .25 & .19 & 2\pi & .20 \\ 5.43 & .43 & .07 & .07 & .19 & 2\pi \end{bmatrix} \begin{bmatrix} c_{P_1} \\ c_{P_2} \\ c_{P_3} \\ c_{P_4} \\ c_{P_5} \\ c_{P_6} \end{bmatrix} = \begin{bmatrix} 0.24 \\ -2.01 \\ 3.85 \\ 8.31 \\ -1.17 \\ -1.47 \end{bmatrix} \quad (28)$$

Notice that the matrix is unchanged from the $\alpha = 0^\circ$ matrix, since its elements depend only on the relation between the various points on the body. Of course, for different Mach numbers the matrix changes, but it is not angle-of-attack dependent.

The angle of attack does significantly alter the RHS vector of the system of equations. This change results in the solution presented in figure 14. The large jump in pressure across the trailing edge is representative of flows over airfoils

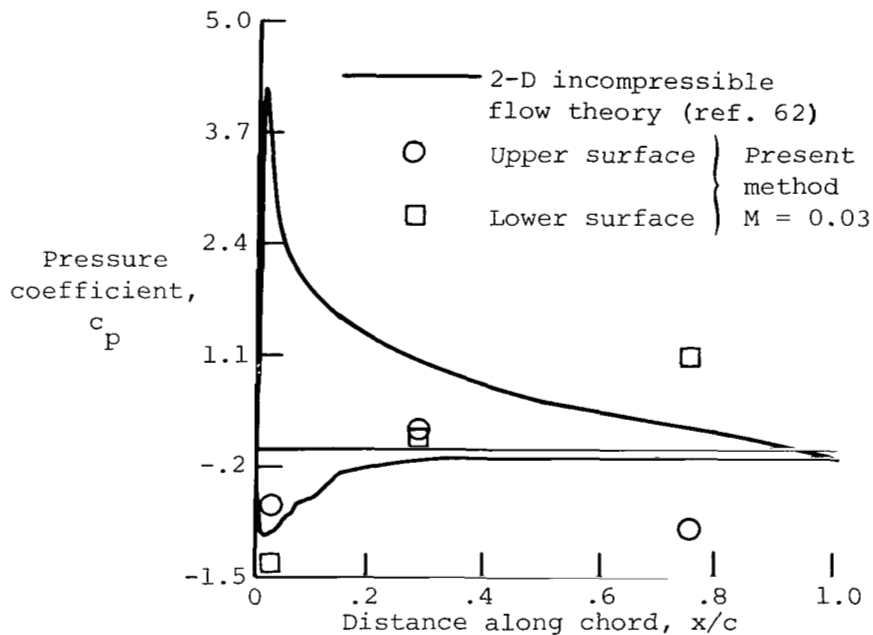


Figure 14.- Pressure distribution on simple six-element airfoil when $\alpha = 10^\circ$.

before applying a Kutta condition. Satisfying the Kutta condition means forcing the pressure on the upper and lower surfaces to be equal at the trailing edge. To understand how to accomplish this, one must remember that the Kutta condition, as stated earlier, forces the flow at the trailing edge to be as it was when the airfoil was

at $\alpha = 0^\circ$, at which the conditions on the upper and lower surfaces were the same. The only difference in the system of equations though is the RHS vector. When $\alpha = 0^\circ$, $b_1 = b_6$, $b_2 = b_5$, and $b_3 = b_4$, but now these no longer hold true. However, they do illustrate a method of applying a Kutta condition. If $b_1 = b_6$ were enforced for the system, then the trailing edge of the airfoil would experience the same flow on the upper and lower surfaces. Therefore, in equations (28) replace b_1 and b_6 by

$$b'_1 = b'_6 = \frac{b_1 + b_6}{2}$$

which gives

$$\begin{bmatrix} 2\pi & 0.19 & 0.07 & 0.07 & 0.43 & 5.43 \\ 0.20 & 2\pi & .19 & .25 & 4.92 & .61 \\ .17 & .28 & 2\pi & .10 & .82 & .22 \\ .22 & .82 & .10 & 2\pi & .28 & .17 \\ .61 & 4.92 & .25 & .19 & 2\pi & .20 \\ 5.43 & .43 & .07 & .07 & .19 & 2\pi \end{bmatrix} \begin{bmatrix} c_{p_1} \\ c_{p_2} \\ c_{p_3} \\ c_{p_4} \\ c_{p_5} \\ c_{p_6} \end{bmatrix} = \begin{bmatrix} -0.61 \\ -2.01 \\ 3.85 \\ 8.31 \\ -1.17 \\ -.61 \end{bmatrix} \quad (29)$$

The solution of this system is shown in figure 15. By using averaged values for b_i near the trailing edge, a Kutta-type condition was enforced which produces a net force on the body due to the difference in pressure on the upper and lower surfaces.

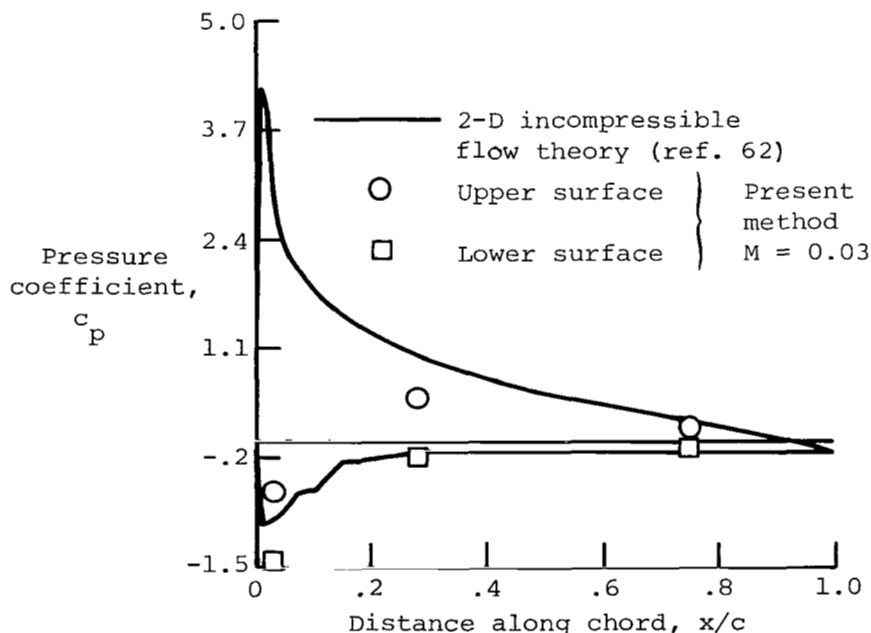


Figure 15.- Pressure distribution on simple six-element airfoil when $\alpha = 10^\circ$ with Kutta condition.

One aspect of this conditioning technique that was not illustrated very well by this simple example is that it must be applied over a large portion of the chord. In this example the trailing-edge panel was very large, covering 50 percent of the chord. If many elements had been used along the chord, this conditioning would have had to be applied to several, unlike velocity-potential panel methods where vorticity is distributed inside the body. When using the vorticity method, one must apply a Kutta condition only on the panels adjacent to the trailing edge because the vorticity tends to couple strongly the leading- and trailing-edge algebraic equations (in fact the equations for the whole airfoil). When using the pressure formulation, there is no strong coupling between the leading and trailing edges. In fact, the panels on the upper and lower surfaces of the trailing edge affect each other so strongly that they are almost unaffected even by adjacent panels. Thus, applying the Kutta condition only to the single pair of panels at the trailing edge would have almost no effect on the next set of panels forward from the trailing edge. Therefore, the conditioning must be applied to a large section on the aft of the airfoil. From preliminary studies on uncambered, symmetric airfoils, it has been determined that this conditioning of the RHS vector must be applied to all panels from the trailing edge to the thickest part of the airfoil. Thus, for an NACA 0012 airfoil, with many panels along the chord, one would condition the vector over 70 percent of the chord, since this airfoil is thickest at 70 percent of the chord (from the trailing edge). As an example, if one modeled the airfoil by 10 panels on the upper surface and 10 on the lower, where each panel covered 10 percent of the chord, the vector would be conditioned as follows:

$$b'_1 = b'_{20} = \frac{b_1 + b_{20}}{2}$$

$$b'_2 = b'_{19} = \frac{b_2 + b_{19}}{2}$$

⋮

$$b'_7 = b'_{14} = \frac{b_7 + b_{14}}{2}$$

The above technique has an effect completely analogous to that of using Van Holten's suggestion, except that its implementation is much simpler because the body is not considered to be deformed in any manner.

It is also interesting to note that using the displacement thickness effect also conditions the equations in a similar manner. By thickening the body by an amount equal to the displacement thickness, one moves the two trailing-edge panels (upper and lower surfaces) farther apart. This tends to move the values of b_i on the RHS of equations (28) closer together. The larger the displacement thickness, the closer the values become.

V. RESULTS

This section presents numerical results for several different types of bodies in various combinations of rectilinear and angular motion. Using the computer program described in section III, the surface pressure was calculated for prolate ellipsoids, wings, and rotating blades. These different types of bodies were used to illustrate the generality of the method.

A. Prolate Ellipsoids

Prolate ellipsoids with fineness ratios of 0.05, 0.10, and 0.25 were modeled in low-speed motion. These were chosen because of the availability of theoretical (incompressible) and experimental results with which to compare (ref. 64).

First, the results for a 5-percent-thick ellipsoid are presented. The paneling used is illustrated in figure 16. There were 264 panels and symmetry was not exploited. If one takes advantage of the numerous planes of symmetry, the number of computations and the amount of storage can be reduced substantially. Panels were concentrated near the ends of the ellipsoid because of the extremely rapid change in pressure occurring there. Remember that the pressure is assumed constant over each panel.

The numerical and experimental results are compared in figure 17, which is a graph of pressure coefficient versus axial distance. The solid line represents experimental results (ref. 64), and the symbols represent the current numerical results. Agreement is generally good except near the stagnation point. Poor agreement there is expected because of the use of linearized theory. Near the ends of the ellipsoid the flow is essentially that for a blunt body, and linearized theory is usually valid to within a few percent of the chord from the leading edge (ref. 44, p. 209). For more detailed descriptions of the flow near the stagnation point one could use the methods of Van Dyke (ref. 65) or include the quadrupole terms, which include the nonlinear effects, in the present formulation. Neither would be trivial to incorporate into the current scheme.

Figure 18 shows the paneling used for a 10-percent-thick ellipsoid, and results similar to those just discussed are shown in figure 19. Figures 20 and 21 show the same information for a 25-percent-thick ellipsoid. From these figures it is obvious that the nonlinear terms become more and more important for the thicker bodies. Of course, these are extreme examples in that most aerodynamic shapes have thicknesses of 15 percent or less, especially those designed for higher speeds. For a detailed discussion of the implications of nonlinearity in the pressure formulation, see section I. Further, ellipsoids are a severe test of linear theory because of their blunt ends. Much more accurate results would be expected for shapes such as ogives and wings.



Figure 16.- Paneling used to model 5-percent-thick ellipsoid.

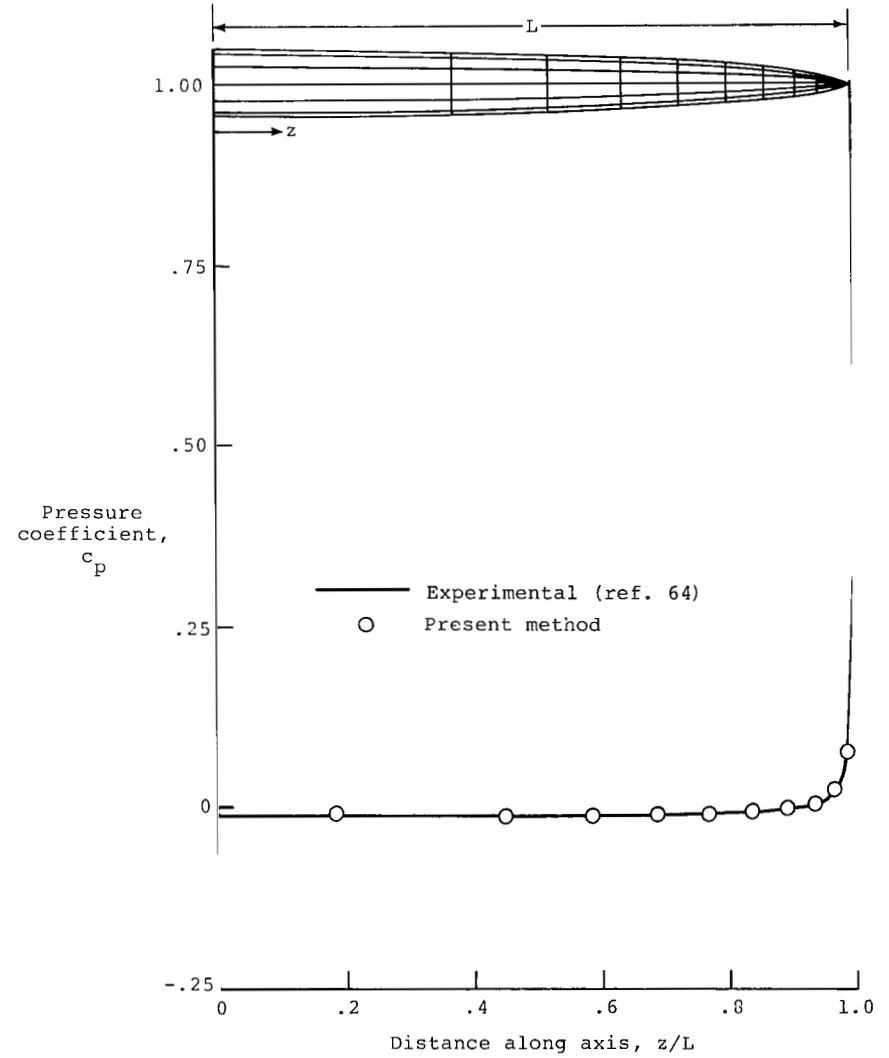


Figure 17.- Pressure distribution on 5-percent-thick ellipsoid.

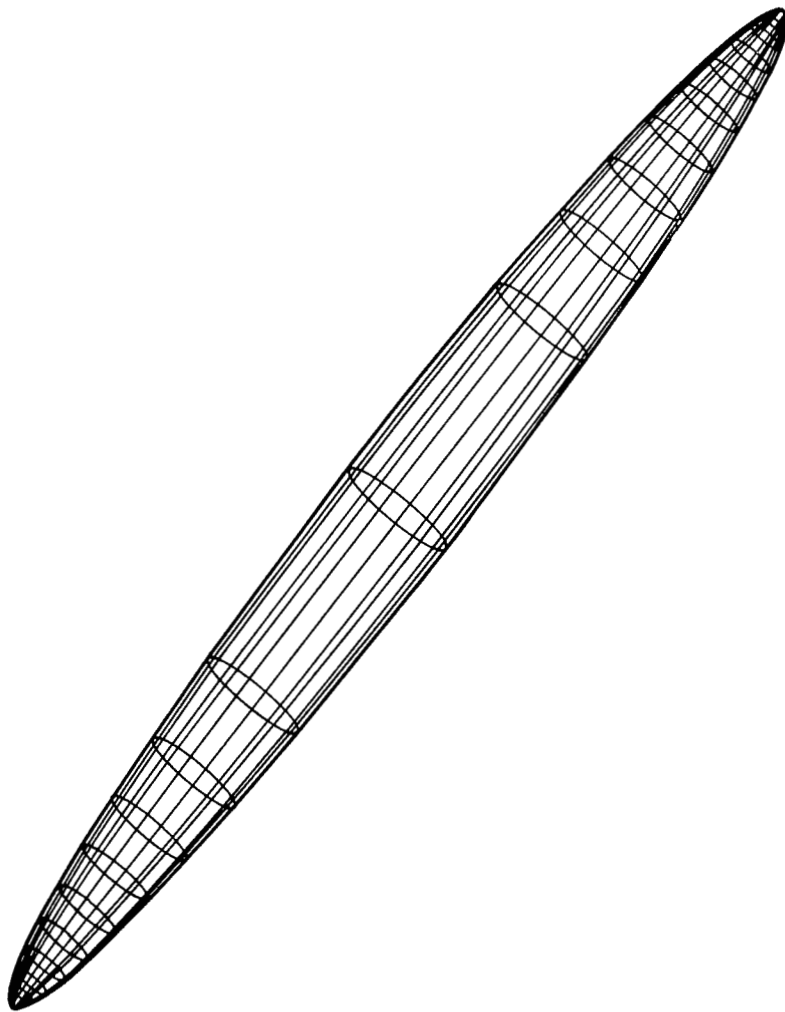


Figure 18.- Paneling used to model 10-percent-thick ellipsoid.

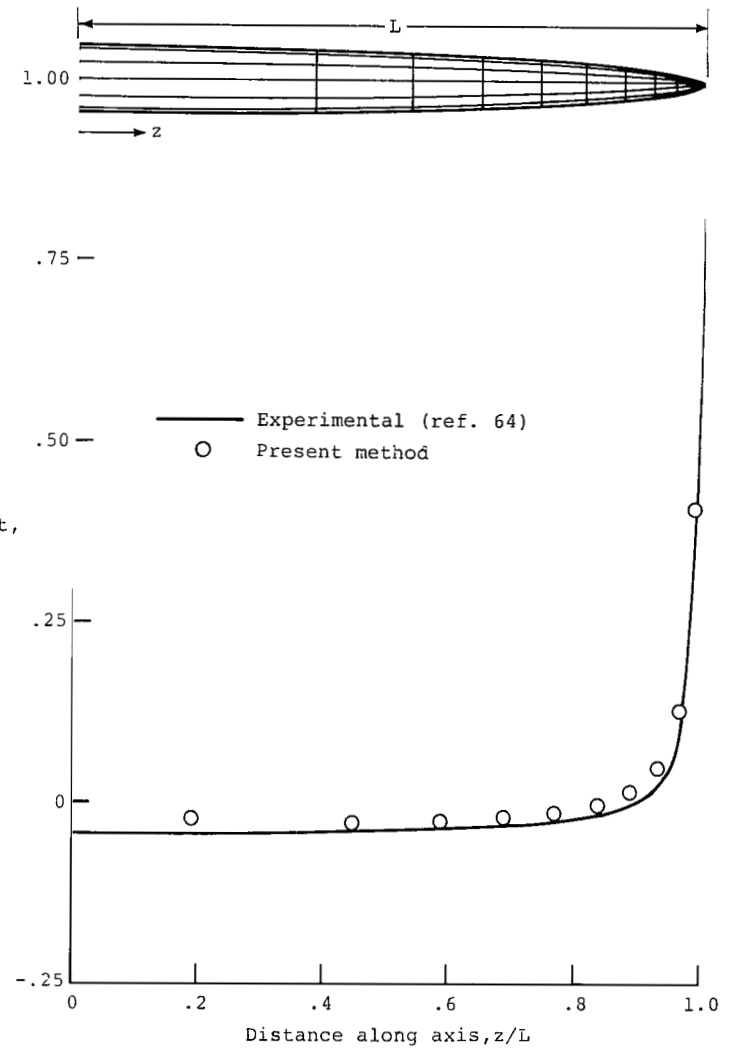


Figure 19.- Pressure distribution on 10-percent-thick ellipsoid.

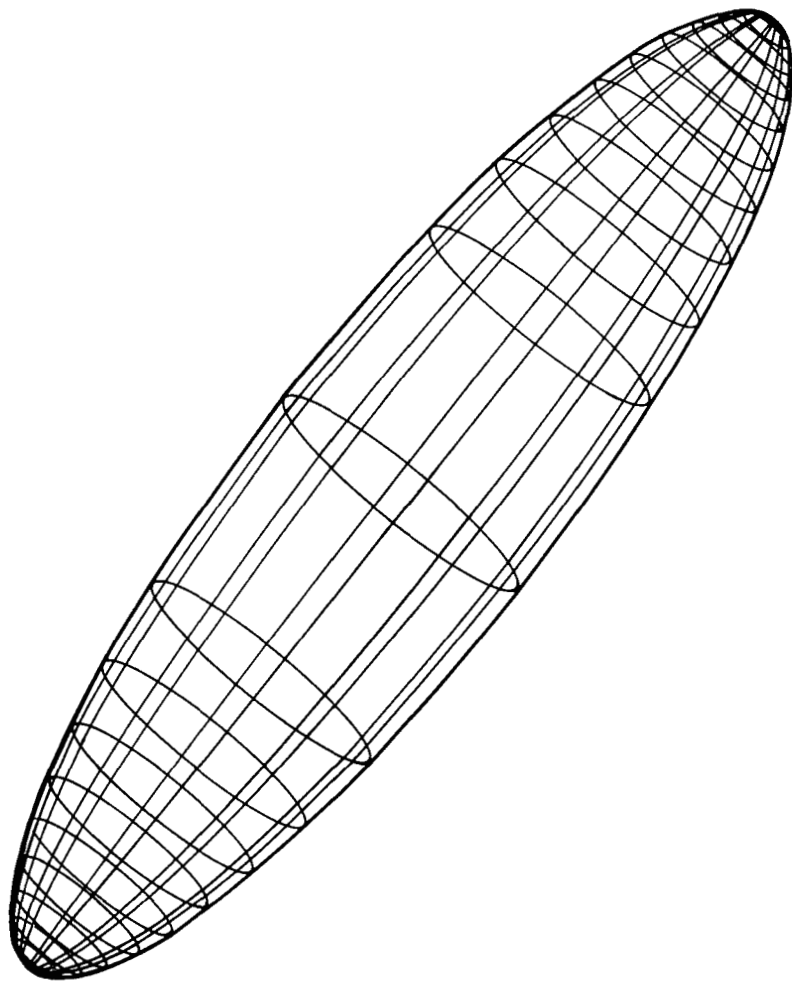


Figure 20.- Paneling used to model 25-percent-thick ellipsoid.

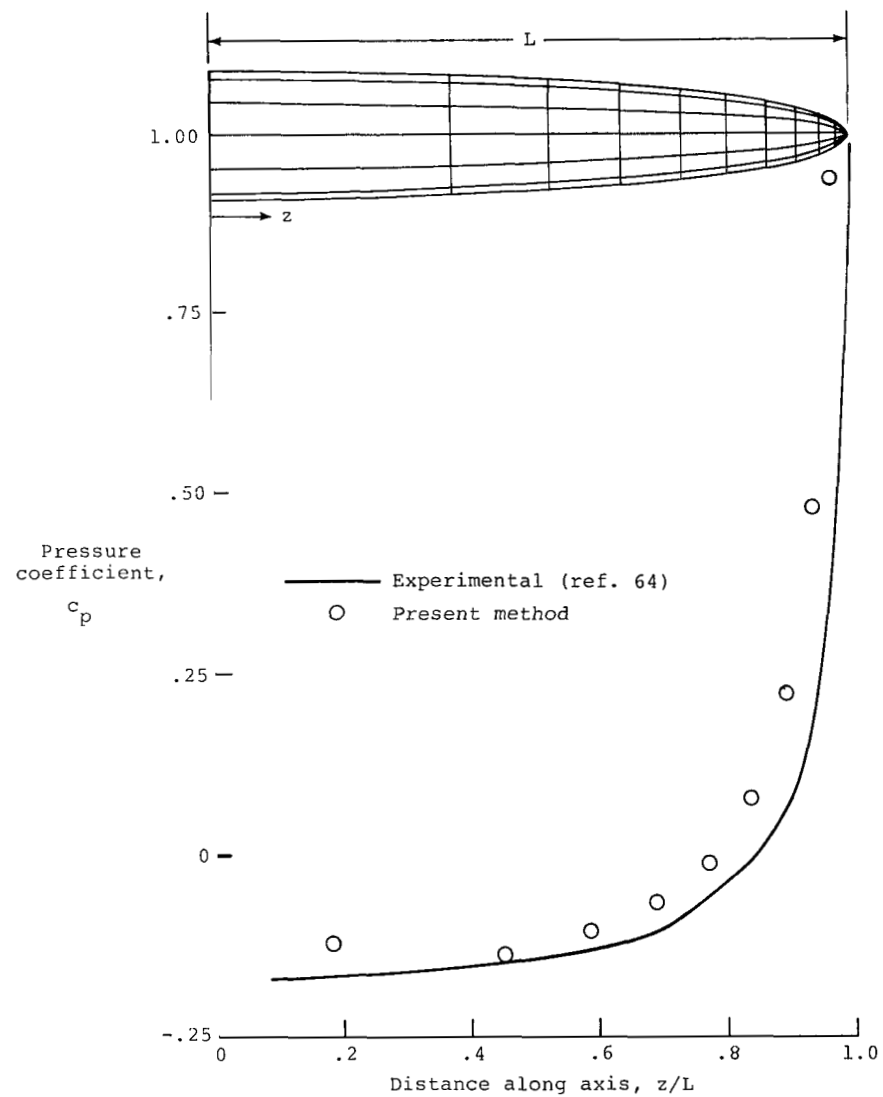


Figure 21.- Pressure distribution on 25-percent-thick ellipsoid.

B. Finite Wing

The next example is a finite wing with an NACA 0008 cross section and an aspect ratio of 5. The paneling used and its cross section are shown in figure 22. There were 242 panels with no special precautions taken near the tip. In fact, the tips are not paneled at all; they are actually open. Including these panels had an insignificant effect on the panels away from the tips. And since this section compares numerical results with two-dimensional section airfoil theory, only results from the center of this finite wing are presented.

The numerical results from the program described in section III are presented in figure 23. Also shown are two-dimensional potential theory results (incompressible) (ref. 62). The numerical results were obtained for a Mach number of 0.01 and compare very well with the theoretical results. The finite aspect ratio may account for the numerical results being slightly lower than the theoretical curve. The numerical results for $M = 0.06$ are also included. The pressure coefficients are higher than those at $M = 0.01$.

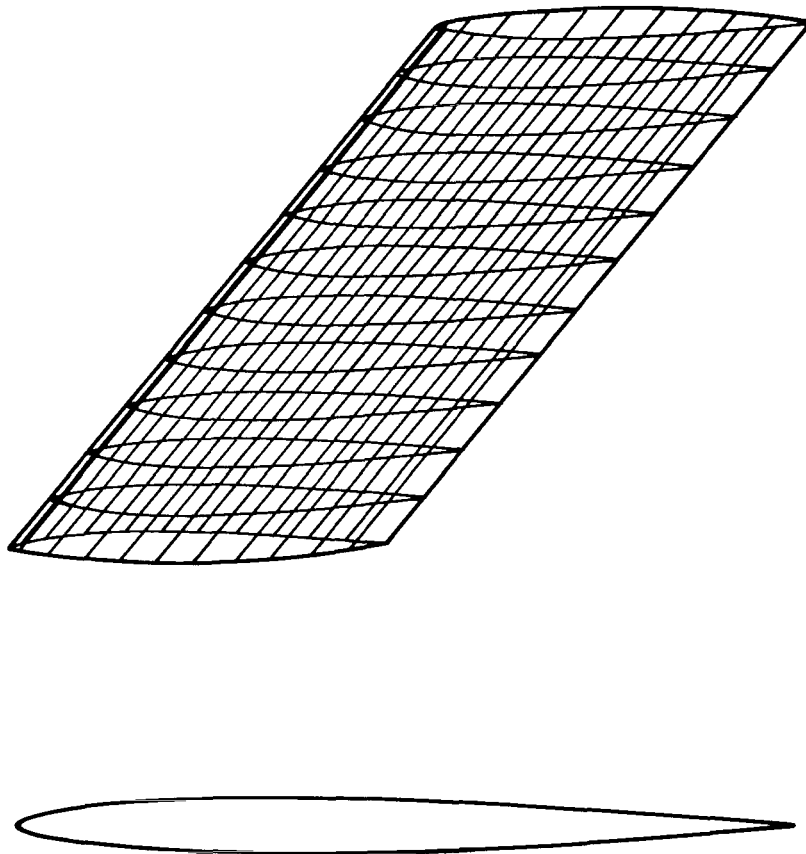


Figure 22.- Paneling used to model NACA 0008 wing.

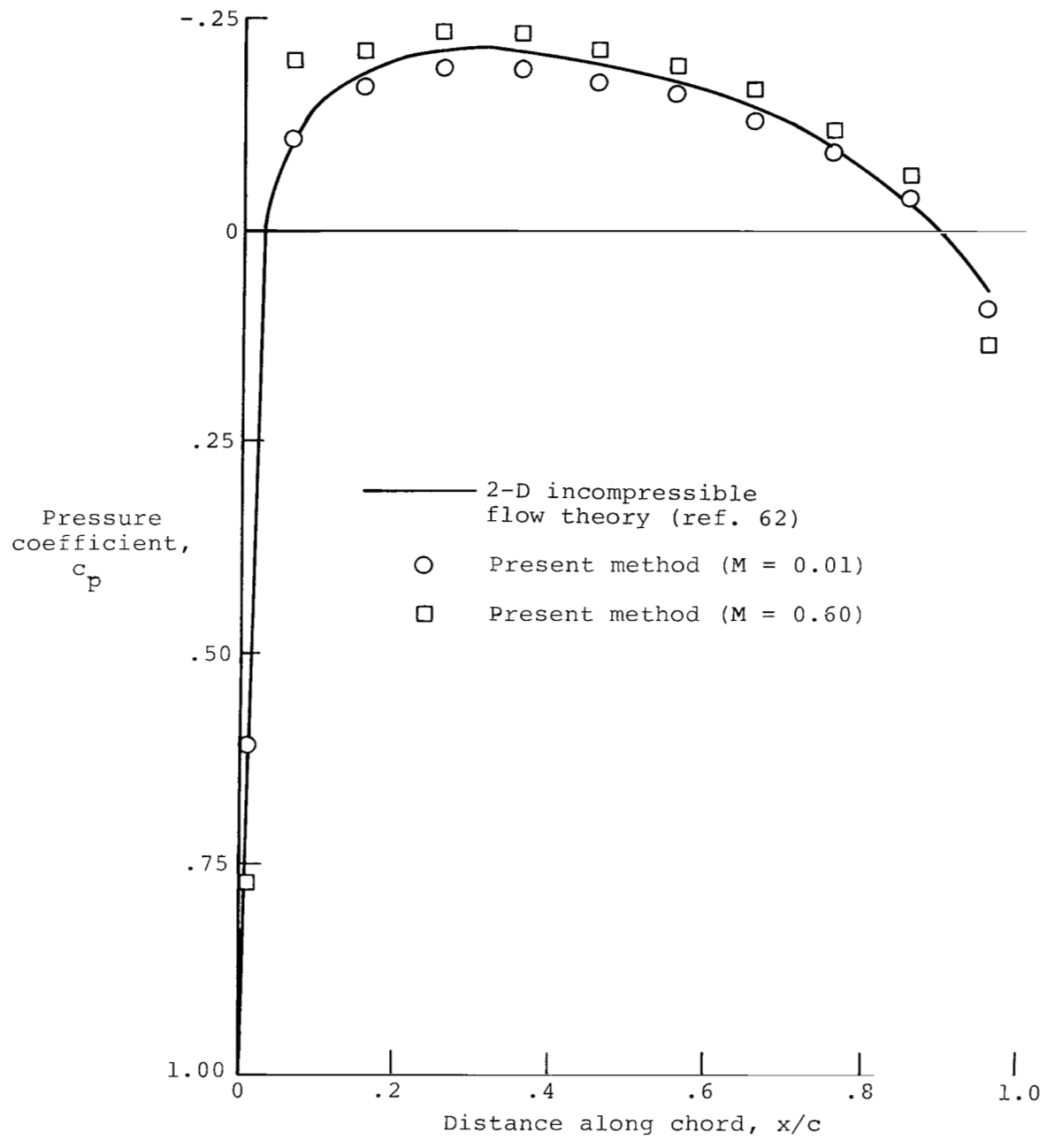


Figure 23.- Pressure distribution on NACA 0008 wing.

C. Helicopter Rotor Blade

In this section numerical results are presented for a rotating NACA 0012 blade. This airfoil section is common in helicopter applications. The results are compared with the experiments of Gray et al. (ref. 66).

The blade was approximated by 264 finite panels as shown in figures 24 and 25. Panel sizes were decreased smoothly from root to tip. Blade length was 6.5 chord lengths. Tip Mach number was 0.25 and angle of attack was zero.

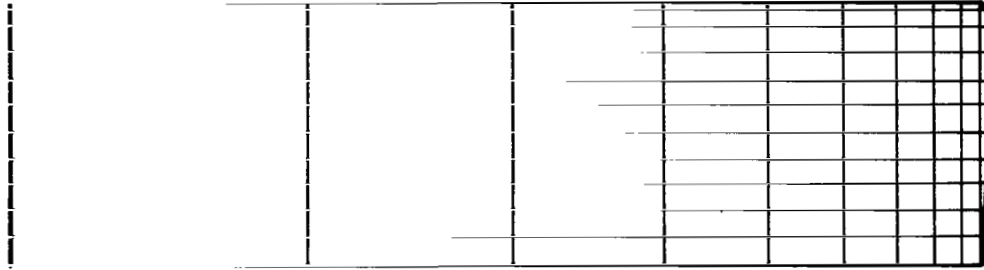


Figure 24.- Planform view of paneling used to model NACA 0012 helicopter rotor.

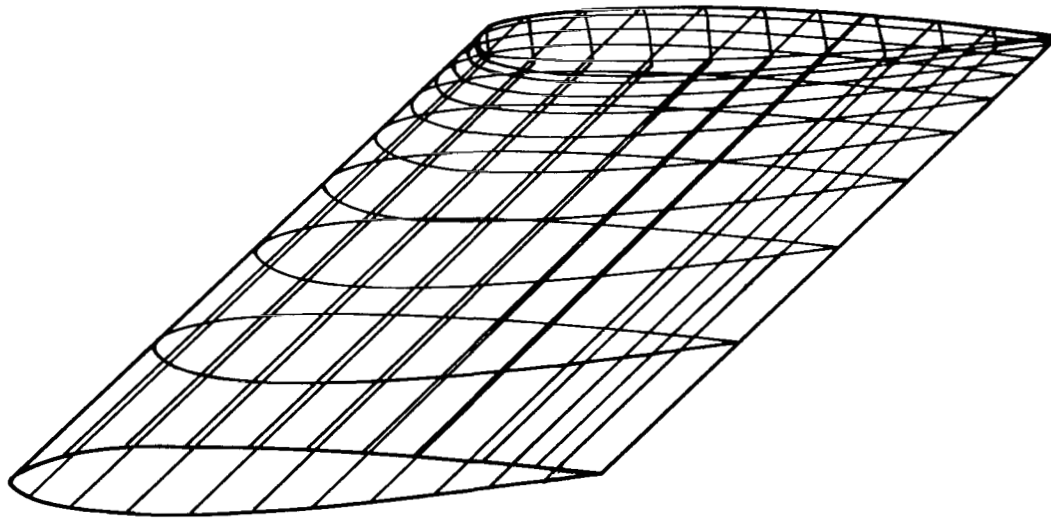


Figure 25.- Paneling used to model NACA 0012 helicopter rotor.

Figures 26, 27, and 28 compare the variation in the pressure coefficient along the chord for three spanwise locations: 94, 98, and 99.5 percent. The solid line represents two-dimensional airfoil theory (ref. 62). The circular symbols are experimental results (ref. 66) and the squares are the present numerical calculations. The leading edge is obviously at $x/c = 0$.

These results agree well with experiment. Notice how close to the two-dimensional theory the results are at the 94-percent span location. Three-dimensional effects become obvious as one moves closer to the tip. Of course at the leading edge the well-known square-root singularity appears. The solution in this region can be approximated with the methods described in reference 65.

Figures 29, 30, and 31 present similar results for the blade at an angle of attack. The concepts discussed in section IV allow the calculation of surface pressures on lifting bodies. As described there, the inhomogeneous terms of the system of algebraic equations must be conditioned by replacing the inhomogeneous terms (for the panels on the upper and lower surfaces at the trailing edge) by the average of the two values. This must be done for all panels from the trailing edge to the thickest part of the cross section. Here too the numerical results agree well with experiment (solid lines). The circular and square symbols represent the numerical results from the upper and lower surfaces, respectively.

Now, surface pressure calculations from an NACA 0006 rotor at various Mach numbers are presented. Figure 32 shows the pressure coefficient at 94 percent span versus distance along the chord for tip Mach numbers of 0.5, 0.7, and 0.9. The solid curve indicates the two-dimensional section result for incompressible flow. Notice that the numerical results are markedly different from those that would be expected from two-dimensional compressible flow. The Prandtl-Glauert rule indicates that the line should shift upward for increasing Mach number according to

$$c_p = \frac{c_{p_0}}{\sqrt{1 - M^2}}$$

where c_{p_0} is the incompressible pressure coefficient. But because of the highly three-dimensional nature of flow around a rotating blade, this rule does not apply. This is verified by the computational results, which deviate significantly from what the Prandtl-Glauert rule would predict. Note that for large aspect ratio wings in rectilinear motion, the computational method presented herein does predict behavior similar to that of the Prandtl-Glauert rule.

One final point concerns the amount of computation time that was used on these calculations. It is relatively small considering the details obtained and the complexities involved. The most time-consuming case, the NACA 0006 rotor at $M_{tip} = 0.9$, required nearly 40 minutes of CPU time on a CDC CYBER 175 computer. The same blade at $M_{tip} = 0.01$ required 21 CPU minutes. Remember that this was merely a pilot computer program, and the efficiency could be enhanced by optimizing the code.

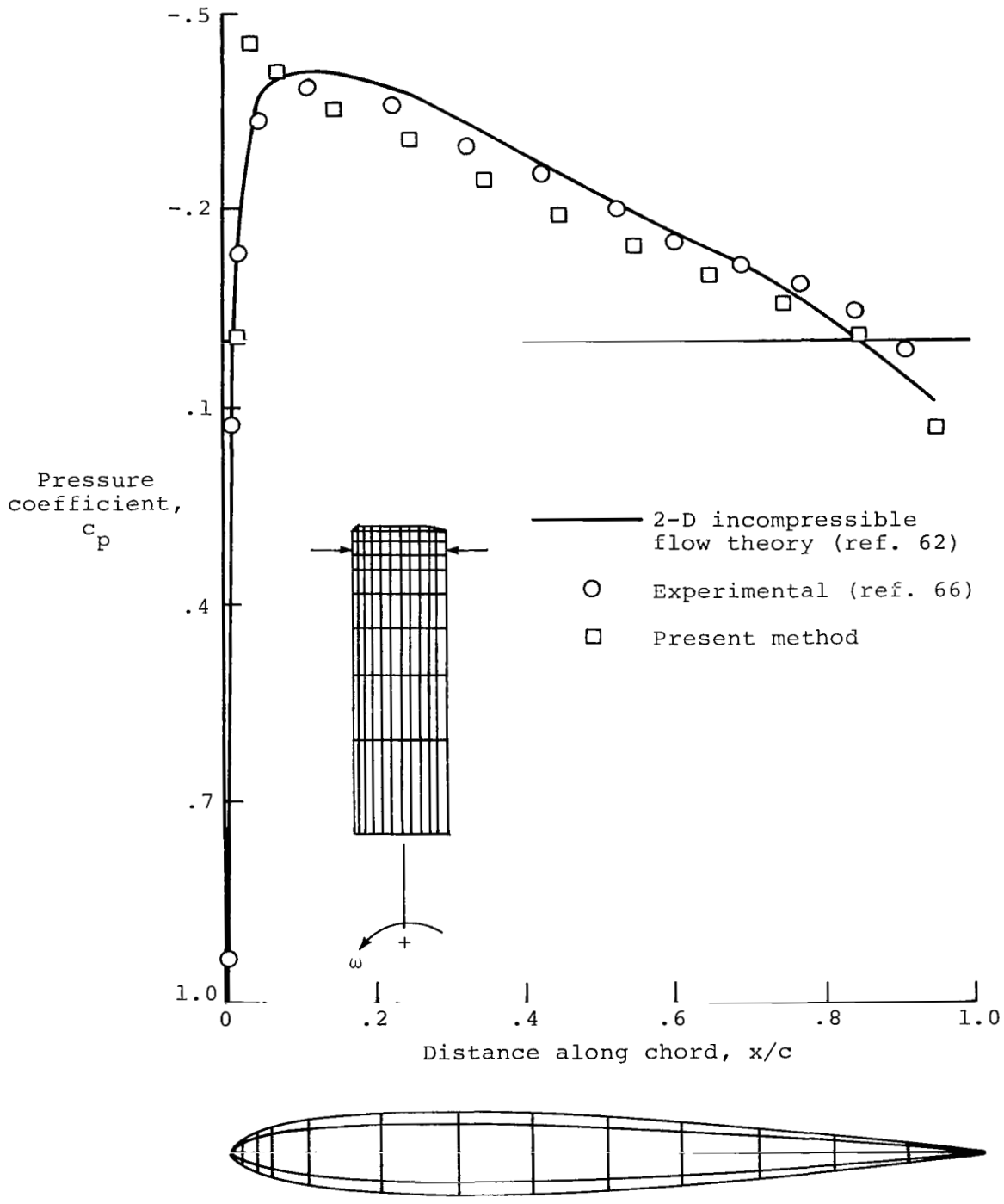


Figure 26.- Pressure distribution on NACA 0012 rotor at 94 percent span when $\alpha = 0^\circ$. $M_{tip} = 0.25$.

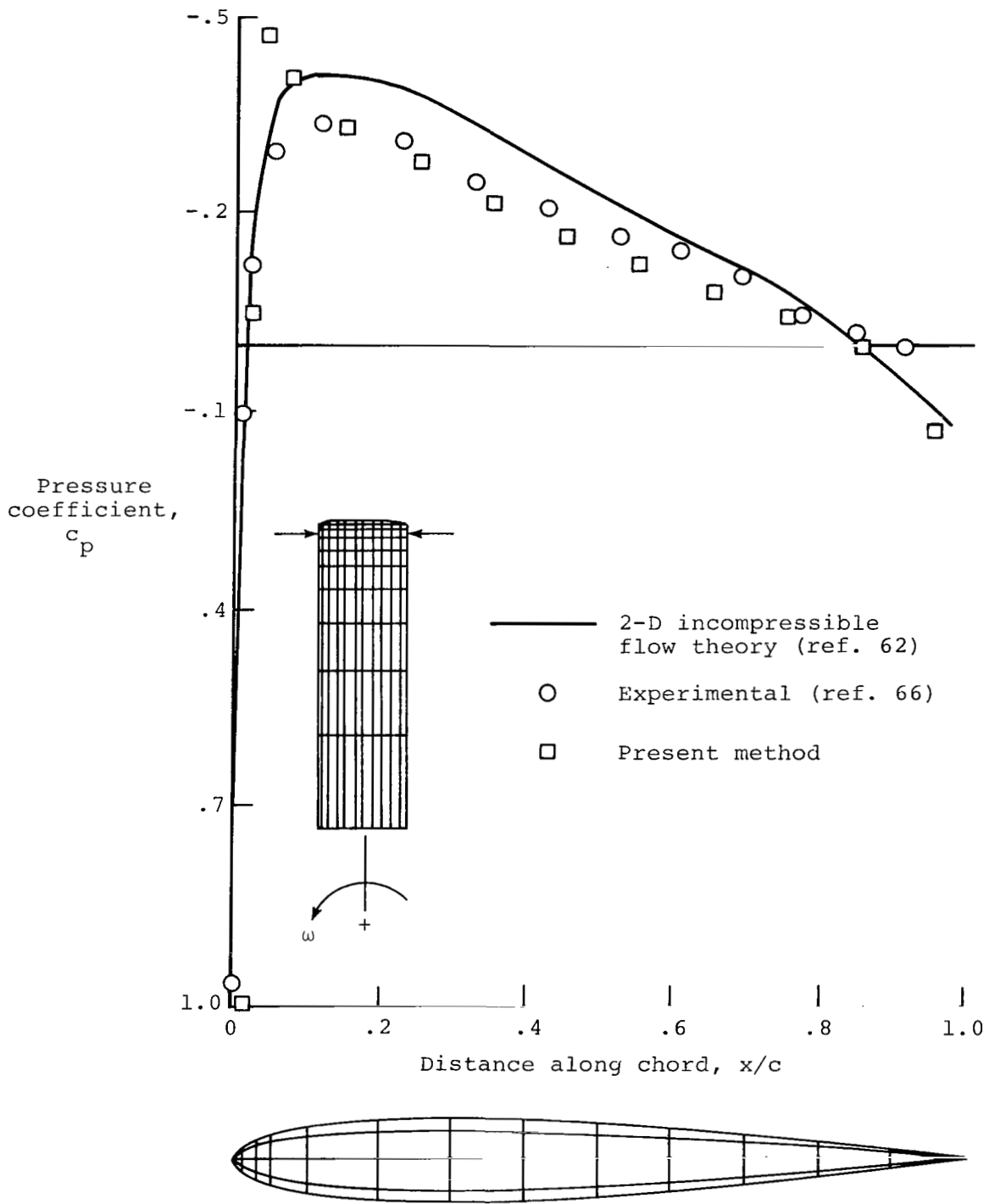


Figure 27.- Pressure distribution on NACA 0012 rotor at 98 percent span when $\alpha = 0^\circ$. $M_{tip} = 0.25$.

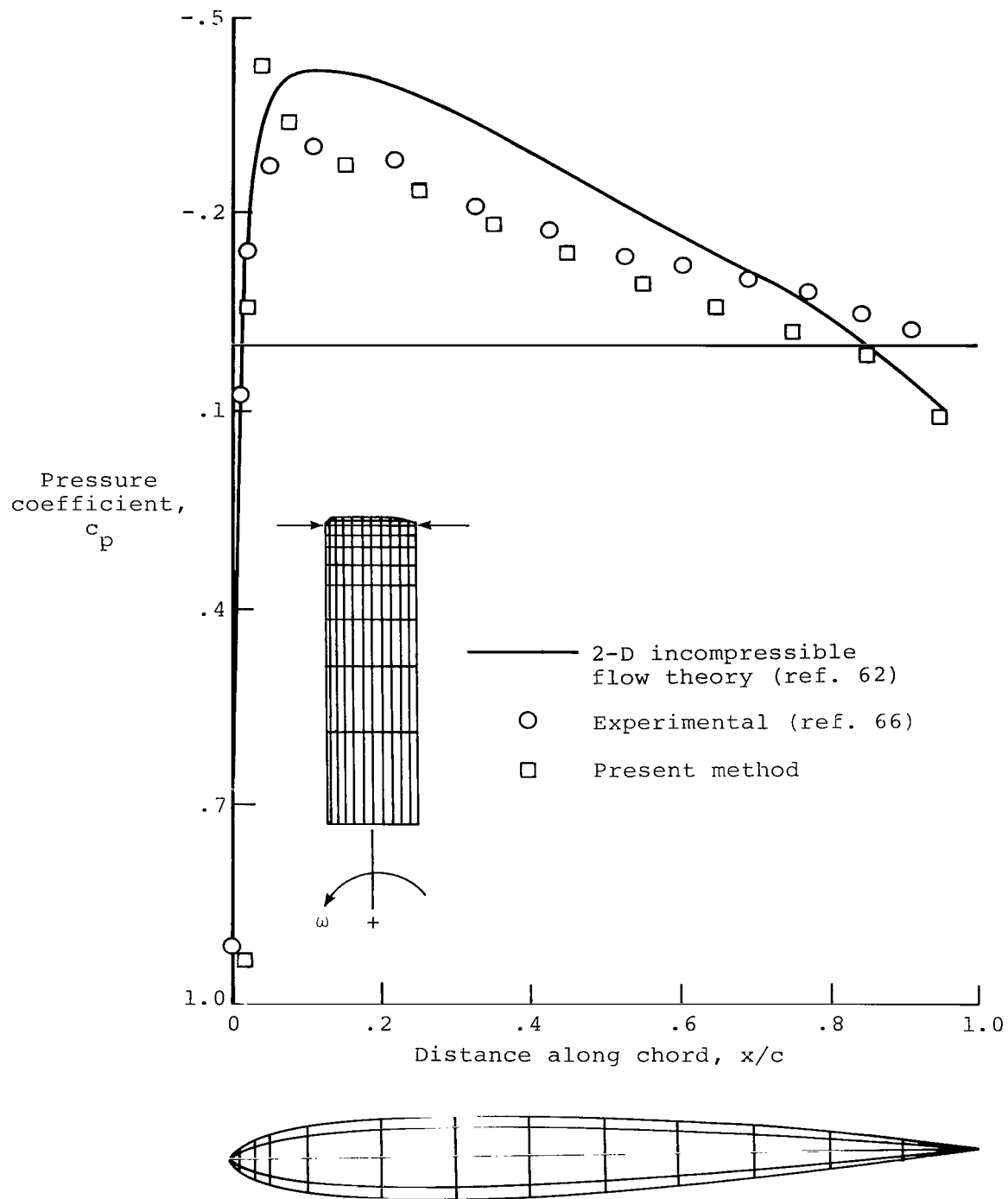


Figure 28.- Pressure distribution on NACA 0012 rotor at 99.5 percent span when $\alpha = 0^\circ$. $M_{tip} = 0.25$.

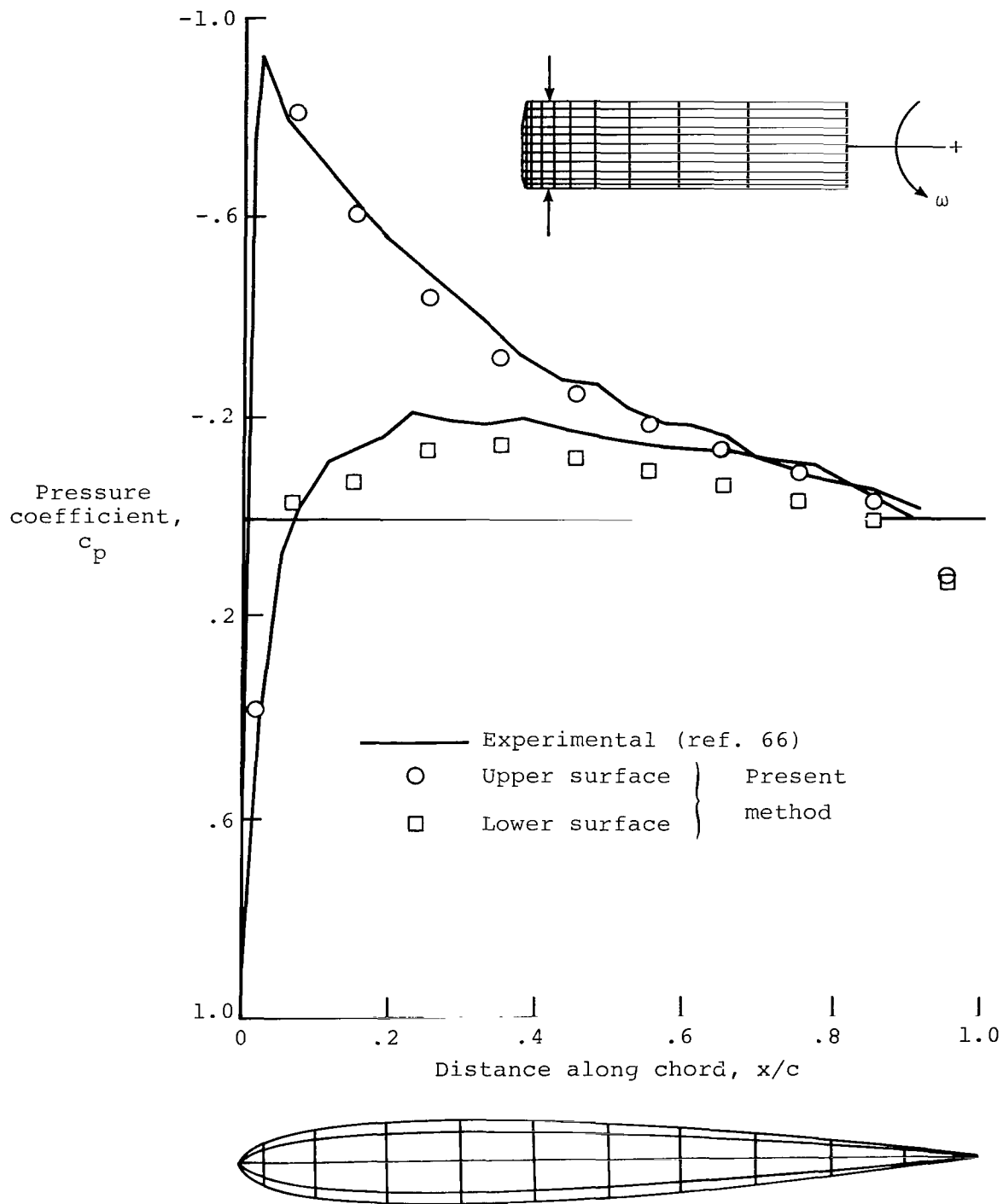


Figure 29.- Pressure distribution on NACA 0012 rotor at 94 percent span when $\alpha = 6.18^\circ$. $M_{tip} = 0.25$.

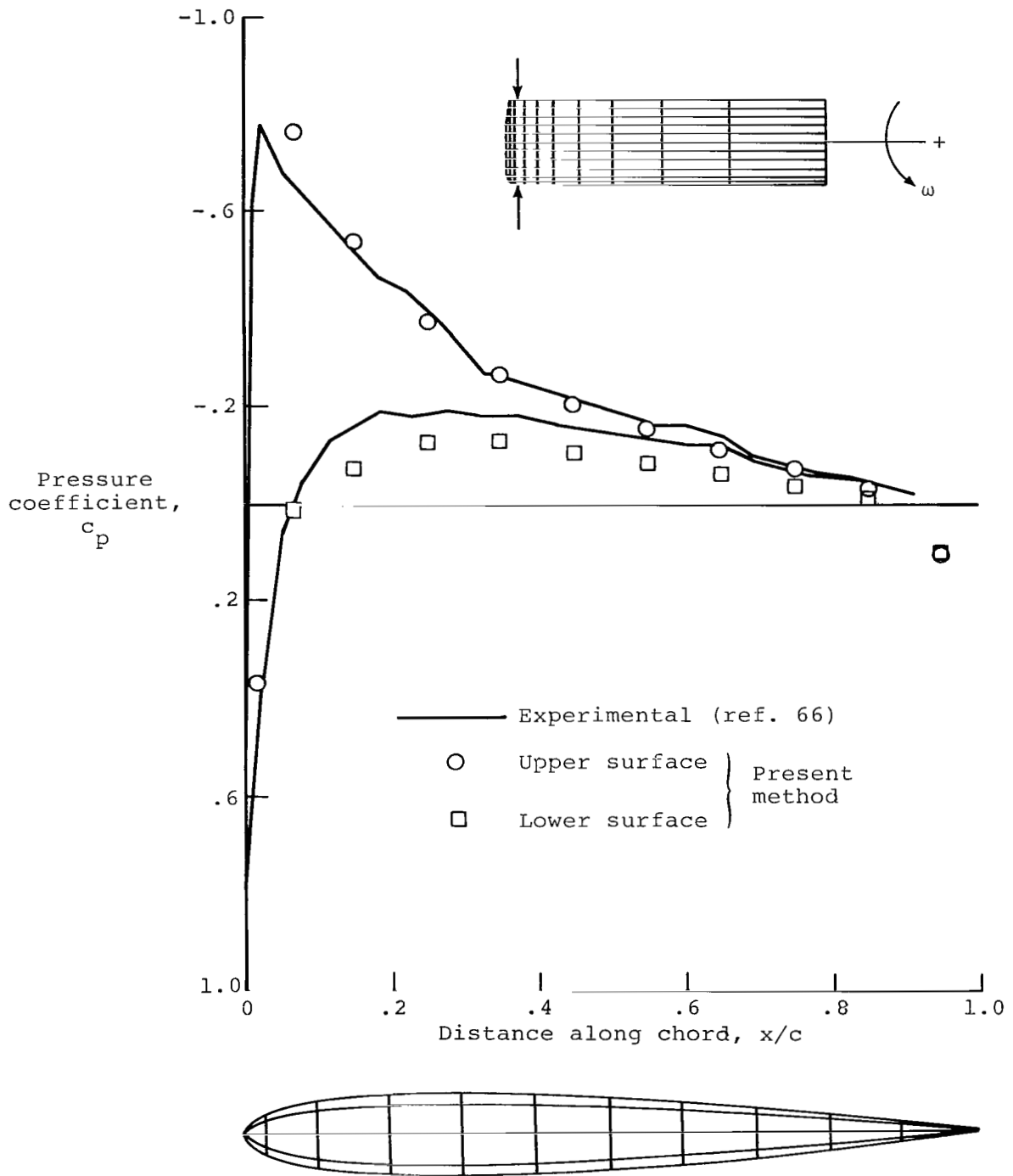


Figure 30.- Pressure distribution on NACA 0012 rotor at 98 percent span when $\alpha = 6.18^\circ$. $M_{tip} = 0.25$.

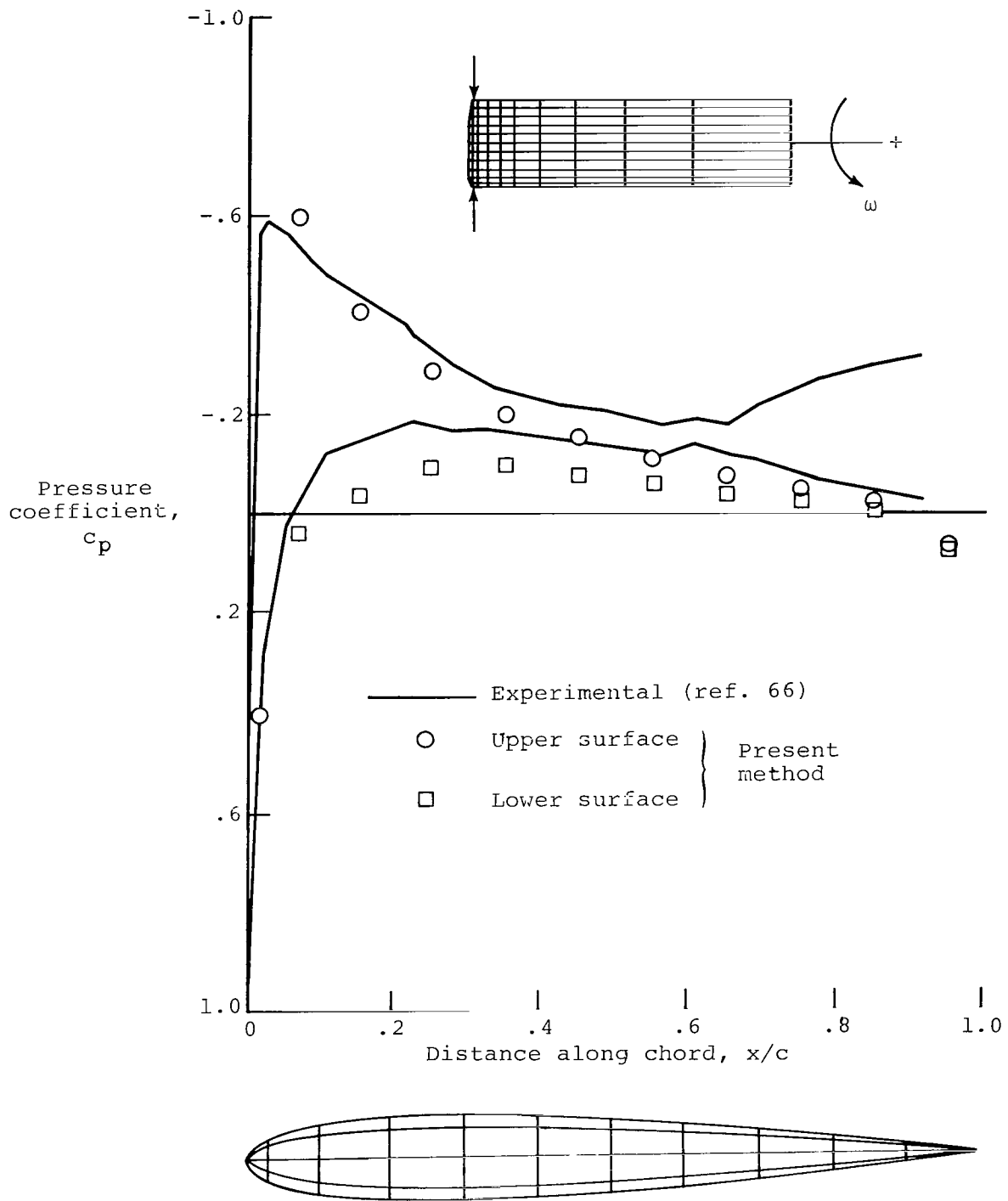


Figure 31.- Pressure distribution on NACA 0012 rotor at 99.5 percent span when $\alpha = 6.18^\circ$. $M_{tip} = 0.25$.

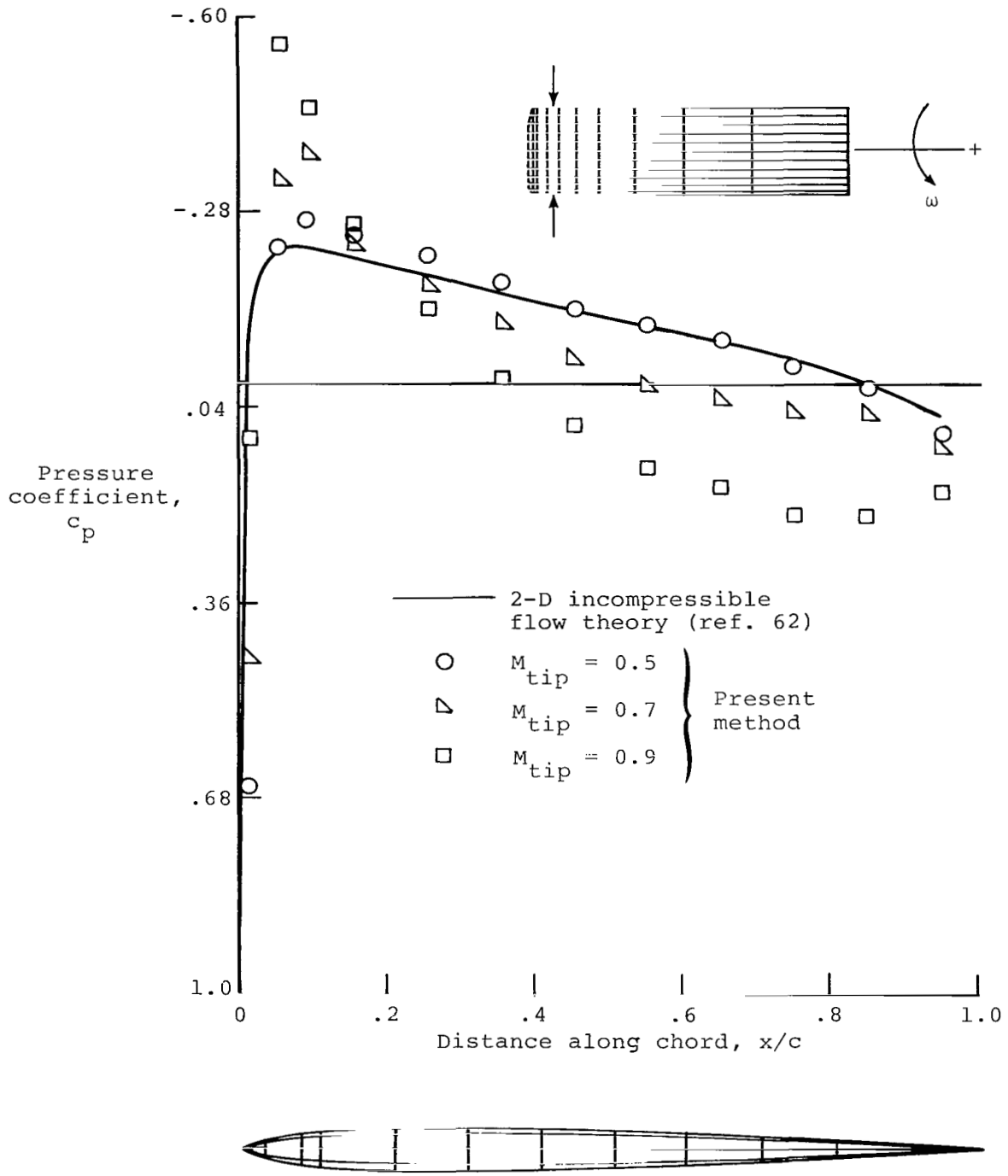


Figure 32.- Pressure distribution on NACA 0006 rotor at 94 percent span for several tip Mach numbers. $\alpha = 0^\circ$.

VI. CONCLUSION

This report describes a method for calculating the surface pressure on arbitrary bodies in compressible flow. It is based on the acoustic analogy approach of Ffowcs Williams and Hawkings and the equations due to Farassat. Its major contributions have been in interpreting Farassat's equation when the observation point is located on the surface of the body and in solving the resulting equation numerically.

Since Farassat's equation is based on linearized, inviscid theory, the method presented here of course has its limitations. These have been pointed out whenever possible in the text. For bodies moving in rectilinear motion there may be more appropriate theories in which some nonlinear effects may be included relatively easily. For bodies such as propellers and helicopter rotors, for which the problem is very complex, the present results are very encouraging. The method is based on first principles and is relatively easy to comprehend, yet it provides an inexpensive way to obtain very useful information. In addition, because the Ffowcs Williams-Hawkings equation does contain viscous and nonlinear terms, there is hope for including these effects in the future.

The method described herein contains several ideas that are somewhat novel to aerodynamic theory. First, compressibility is accounted for exactly as it occurs in nature, in terms of retarded time. Compressibility manifests itself as a finite speed of propagation of disturbances, and in the current theory the distance the signal actually travels is calculated. In the past this was an insurmountable complication; but because of recent advancements in computer technology, it is now possible to model these effects. Furthermore, the effects due to lift are included without recourse to distributions of vorticity. A method is presented for conditioning the final system of algebraic equations (generated by the computer program) to account for lift via a Kutta, or trailing-edge, condition. This conditioning amounts to setting the pressure equal on the upper and lower surface of the trailing edge. Vorticity is not required because the theory is formulated in terms of the pressure.

Langley Research Center
National Aeronautics and Space Administration
Hampton, VA 23665
August 22, 1983

APPENDIX A

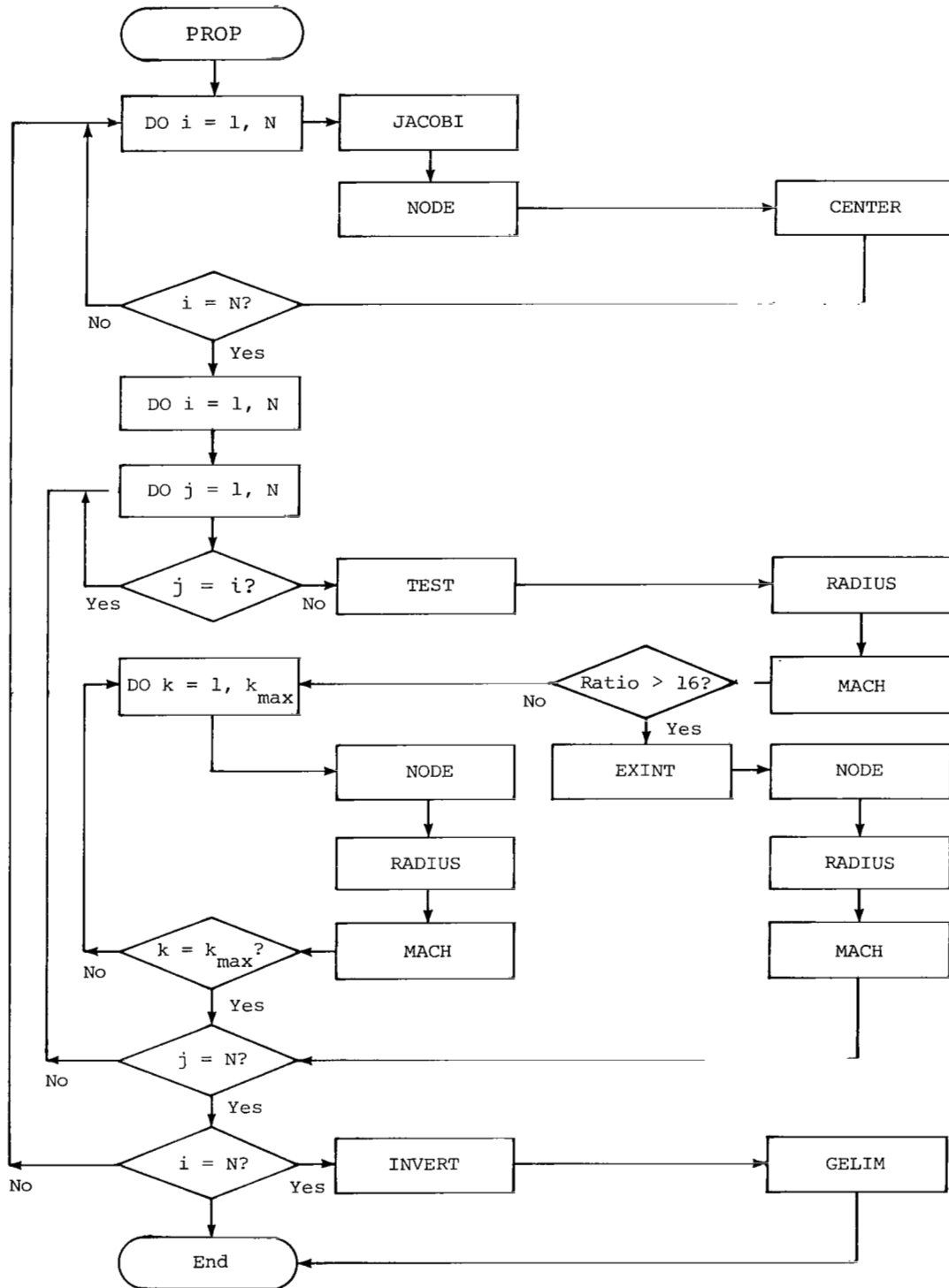
LEGENDRE-GAUSS QUADRATURE FORMULAS

$$\text{Notation: } \int_{-1}^1 f(x) dx = \sum_{i=1}^N H_i f(x_i)$$

Node locations, x_i	Weight coefficients, H_i
N = 2	
0.5773502691 8962576451	(1)0.1000000000 0000000000
N = 3	
0.7745966692 4148337704	0.5555555555 5555555556
0.0000000000 0000000000	0.8888888888 8888888889
N = 4	
0.8611363115 9405257523	0.3478548451 3745385737
0.3399810435 8485626480	0.6521451548 6254614263
N = 5	
0.9061798459 3866399280	0.2369268850 5618908751
0.5384693101 0568309104	0.4786286704 9936646804
0.0000000000 0000000000	0.5688888888 8888888889
N = 6	
0.9324695142 0315202781	0.1713244923 7917034504
0.6612093864 6626451366	0.3607615730 4813860757
0.2386191860 8319690863	0.4679139345 7269104739
N = 7	
0.9491079123 4275852453	0.1294849661 6886969327
0.7415311855 9939443986	0.2797053914 8927666790
0.4058451513 7739716691	0.3818300505 0511894495
0.0000000000 0000000000	0.4179591836 7346938776
N = 8	
0.9602898564 9753623168	0.1012285362 9037625915
0.7966664774 1362673959	0.2223810344 5337447054
0.5255324099 1632898582	0.3137066458 7788728734
0.1834346424 9564980494	0.3626837833 7836198297
N = 10	
0.9739065285 1717172008	(-1)0.6667134430 8688137594
0.8650633666 8898451073	0.1494513491 5058059315
0.6794095682 9902440623	0.2190863625 1598204400
0.4333953941 2924719080	0.2692667193 0999635509
0.1488743389 8163121088	0.2955242247 1475287017
N = 12	
0.9815606342 4671925069	(-1)0.4717533638 6511827195
0.9041172563 7047485668	0.1069393259 9531843096
0.7699026741 9430468704	0.1600783285 4334622633
0.5873179542 8661744730	0.2031674267 2306592175
0.3678314989 9818019375	0.2334925365 3835480876
0.1252334085 1146891547	0.2491470458 1340278500
N = 16	
0.9894009349 9164993260	(-1)0.2715245941 1754094852
0.9445750230 7323257608	(-1)0.6225352393 8647892863
0.8656312023 8783174388	(-1)0.9515851168 2492784810
0.7554044083 5500303390	0.1246289712 5553387205
0.6178762444 0264374845	0.1495959888 1657673208
0.4580167776 5722738634	0.1691565193 9500253819
0.2816035507 7925891323	0.1826034150 4492358887
(-1)0.9501250983 7637440185	0.1894506104 5506849629

APPENDIX B

FLOWCHART OF SUBROUTINES IN COMPUTER PROGRAM



REFERENCES

1. Gatzen, Bernard S.: Advanced Turboprop Propulsion Technology. Propeller Performance and Noise, VKI-LS 1982-08, Volume 2, Von Karman Inst. Fluid Dyn., May 1982.
2. Arkell, Basil; and Taylor, John W. R.: Helicopters and VTOL Aircraft Work Like This, Fourth rev. ed. J. M. Dent & Sons Ltd. (London), 1972.
3. Farassat, F.: Linear Acoustic Formulas for Calculation of Rotating Blade Noise. AIAA J., vol. 19, no. 9, Sept. 1981, pp. 1122-1130.
4. Lighthill, M. J.: On Sound Generated Aerodynamically. I. General Theory. Proc. R. Soc. London, ser. A, vol. 211, no. 1107, Mar. 20, 1952, pp. 564-587.
5. Lighthill, M. J.: On Sound Generated Aerodynamically. II. Turbulence as a Source of Sound. Proc. R. Soc. London, ser. A, vol. 222, no. 1148, Feb. 23, 1954, pp. 1-32.
6. Ffowcs Williams, J. E.; and Hawkings, D. L.: Sound Generation by Turbulence and Surfaces in Arbitrary Motion. Philos. Trans. R. Soc. London, ser. A, vol. 264, no. 1151, May 8, 1969, pp. 321-342.
7. Farassat, F.: Advanced Theoretical Treatment of Propeller Noise. Propeller Performance and Noise, VKI-LS 1982-08, Volume I, Von Karman Inst. Fluid Dyn., May 1982.
8. Farassat, F.: Theory of Noise Generation From Moving Bodies With an Application to Helicopter Rotors. NASA TR R-451, 1975.
9. Prandtl, L.: Beitrag zur Theorie der tragenden Fläche. Z. Angew. Math. & Mech., Bd. 16, Heft 6, Dec. 1936, pp. 360-361.
10. Küssner, H. G.: General Airfoil Theory. NACA TM 979, 1941.
11. Kondo, Kazuo: On the Potential-Theoretical Fundamentals of the Aerodynamics of Screw Propellers at High Speed. J. Fac. Eng., Univ. Tokyo, vol. XXV, no. 1, Jan. 1957, pp. 1-39.
12. Van Holten, Th.: The Computation of Aerodynamic Loads on Helicopter Blades in Forward Flight, Using the Method of the Accelerationpotential. Rep. VTH-189, Tech. Hogeschool Delft Vliegtuigbouwkunde, Mar. 1975.
13. Dat, Rolland: Lifting Surface Theory Applied to Fixed Wings and Propellers. ESRO-TT-90, 1973.
14. Pierce, Allan D.: Acoustics - An Introduction to Its Physical Principles and Applications. McGraw-Hill, Inc., c.1981.
15. Goldstein, Sydney: On the Vortex Theory of Screw Propellers. Proc. R. Soc. London, ser. A, vol. CXXIII, Apr. 1929, pp. 440-465.
16. Lock, C. N. H.: The Application of Goldstein's Theory to the Practical Design of Airscrews. R. & M. No. 1377, British A.R.C., 1932.

17. Morino, Luigi: A General Theory of Unsteady Compressible Potential Aerodynamics. NASA CR-2464, 1974.
18. Zienkiewicz, O. C.: The Finite Element Method. McGraw-Hill Book Co. (UK) Ltd., c.1977, ch. 13.
19. Cruse, T. A.; and Rizzo, F. J., eds.: Boundary-Integral Equation Method: Computational Applications in Applied Mechanics. AMD-Vol. 11, American Soc. Mech. Eng., c.1976.
20. Cruse, Thomas A.: Application of the Boundary-Integral Equation Method to Three Dimensional Stress Analysis. Comput. & Struct., vol. 3, no. 3, May 1973, pp. 509-527.
21. Jaswon, M. A.: Integral Equation Methods in Potential Theory. I. Proc. R. Soc. London, ser. A, vol. 275, no. 1360, Aug. 20, 1963, pp. 23-32.
22. Symm, G. T.: Integral Equation Methods in Potential Theory. II. Proc. R. Soc. London, ser. A, vol. 275, no. 1360, Aug. 20, 1963, pp. 33-46.
23. Lachat, J. C.; and Watson, J. O.: Effective Numerical Treatment of Boundary Integral Equations: A Formulation for Three-Dimensional ElastoStatics. Int. J. Numer. Methods Eng., vol. 10, no. 5, 1976, pp. 991-1005.
24. Schenck, Harry A.: Improved Integral Formulation for Acoustic Radiation Problems. J. Acoust. Soc. America, vol. 44, no. 1, July 1968, pp. 41-58.
25. Copley, Lawrence G.: Fundamental Results Concerning Integral Representations in Acoustic Radiation. J. Acoust. Soc. America, vol. 44, no. 1, July 1968, pp. 28-32.
26. Hess, John L.: Review of Integral-Equation Techniques for Solving Potential-Flow Problems With Emphasis on the Surface-Source Method. Comput. Methods Appl. Mech. & Eng., vol. 5, no. 2, Mar. 1975, pp. 145-196.
27. Hess, John L.: The Problem of Three-Dimensional Lifting Potential Flow and Its Solution by Means of Surface Singularity Distribution. Comput. Methods Appl. Mech. & Eng., vol. 4, no. 3, Nov. 1974, pp. 283-319.
28. Hess, John L.; and Smith, A. M. O.: Calculation of Non-Lifting Potential Flow About Arbitrary Three-Dimensional Bodies. Rep. No. E.S. 40622 (Contract No. Nonr 2722(00)), Douglas Aircraft Co., Inc., Mar. 15, 1962.
29. Hess, John L.: Calculation of Potential Flow About Arbitrary Three-Dimensional Lifting Bodies. Rep. No. MDC J5679-01 (Contract N00019-71-C-0524), McDonnell Douglas Corp., Oct. 1972. (Available from DTIC as AD 755 480.)
30. Lamb, Horace: Hydrodynamics, Sixth ed. Dover Publ., Inc., 1945.
31. Bristow, D. R.; and Hawk, J. D.: Subsonic Panel Method for the Efficient Analysis of Multiple Geometry Perturbations. NASA CR-3528, 1982.

32. Kraus, Werner: Panel Methods in Aerodynamics. Numerical Methods in Fluid Dynamics, H. J. Wirz and J. J. Smolderen, eds., McGraw-Hill Book Co., c.1978, pp. 237-297.
33. Moran, Jack; Tinoco, Edward N.; and Johnson, Forrester T.: User's Manual - Subsonic/Supersonic Advanced Panel Pilot Code. NASA CR-152047, 1978.
34. Sytsma, H. S.; Hewitt, B. L.; and Rubbert, P. E.: A Comparison of Panel Methods for Subsonic Flow Computation. AGARD-AG-241, Feb. 1979.
35. Liepmann, H. W.; and Roshko, A.: Elements of Gasdynamics. John Wiley & Sons, Inc., c.1957.
36. Jones, Robert T.; and Cohen, Doris: High Speed Wing Theory. Princeton Univ. Press, 1960.
37. Morino, Luigi: Steady, Oscillatory, and Unsteady Subsonic and Supersonic Aerodynamics - Production Version (SOUSSA-P 1.1), Volume I - Theoretical Manual. NASA CR-159130, 1980.
38. Yates, E. Carson, Jr.; Cunningham, Herbert J.; Desmarais, Robert N.; Silva, Walter A.; and Drobenko, Bohdan: Subsonic Aerodynamic and Flutter Characteristics of Several Wings Calculated by the SOUSSA P1.1 Panel Method. NASA TM-84485, 1982.
39. Gel'fand, I. M.; and Shilov, G. E. (Eugene Saletan, transl.): Generalized Functions. Volume I - Properties and Operations. Academic Press, 1964.
40. Blackburn, H. W.: Quadrupoles in Potential Flow: Two Model Problems. J. Fluid Mech., vol. 116, Mar. 1982, pp. 507-530.
41. Hanson, D. B.; and Fink, M. R.: The Importance of Quadrupole Sources in Prediction of Transonic Tip Speed Propeller Noise. J. Sound & Vib., vol. 62, no. 1, Jan. 8, 1979, pp. 19-38.
42. Morse, Philip M.; and Feshbach, Herman: Methods of Theoretical Physics. Parts I & II, McGraw-Hill Book Co., Inc., 1953.
43. Farassat, F.: Discontinuities in Aerodynamics and Aeroacoustics: The Concept and Applications of Generalized Derivatives. J. Sound & Vib., vol. 55, no. 2, Nov. 22, 1977, pp. 165-193.
44. Bisplinghoff, Raymond L.; Ashley, Holt; and Halfman, Robert L.: Aeroelasticity. Addison-Wesley Pub. Co., c.1955.
45. Nystrom, Paul A.; and Farassat, F.: A Numerical Technique for Calculation of the Noise of High-Speed Propellers With Advanced Blade Geometry. NASA TP-1662, 1980.
46. Scott, William Taussig: The Physics of Electricity and Magnetism, Second ed. John Wiley & Sons, Inc., c.1966.

47. Baker, Christopher T. H.: The Numerical Treatment of Integral Equations. Oxford Univ. Press, 1977.
48. Leathem, J. G.: Volume and Surface Integrals Used in Physics. Hafner Pub. Co., 1912.
49. Kellogg, Oliver Dimon: Foundations of Potential Theory. Frederick Ungar Pub. Co., 1929. (Also published by Dover Publ., Inc., c.1953.)
50. Mangler, K. W.: Improper Integrals in Theoretical Aerodynamics. Rep. No. Aero. 2424, British R.A.E., June 1951.
51. Woan, C. J.; and Gregorek, G. M.: The Exact Numerical Calculation of Propeller Noise. AIAA Paper 78-1122, July 1978.
52. Gradshteyn, I. S.; and Ryzhik, I. M. (Scripta Technica, Inc., transl.): Table of Integrals, Series, and Products, Corrected & Enlarged ed. Academic Press, Inc., 1980.
53. Watkins, Charles E.; Woolston, Donald S.; and Cunningham, Herbert J.: A Systematic Kernel Function Procedure for Determining Aerodynamic Forces on Oscillating or Steady Finite Wings at Subsonic Speeds. NASA TR R-48, 1959.
54. Landahl, Marten T.; and Stark, Valter J. E.: Numerical Lifting-Surface Theory - Problems and Progress. AIAA J., vol. 6, no. 11, Nov. 1968, pp. 2049-2060.
55. Ashley, Holt; Windall, Sheila; and Landahl, Marten T.: New Directions in Lifting Surface Theory. AIAA J., vol. 3, no. 1, Jan. 1965, pp. 3-16.
56. Ralston, Anthony; and Rabinowitz, Philip: A First Course in Numerical Analysis, Second ed. McGraw-Hill, Inc., c.1978.
57. Hildebrand, Francis B.: Advanced Calculus for Applications, Second ed. Prentice-Hall, Inc., c.1976.
58. Segerlind, Larry J.: Applied Finite Element Analysis. John Wiley & Sons, Inc., c.1976.
59. Subprogram Library. Computer Programming Manual, Volume II. Langley Research Center, NASA, 1975.
60. Moore, Franklin K.: Displacement Effect of a Three-Dimensional Boundary Layer. NACA Rep. 1124, 1953. (Supersedes NACA TN 2722.)
61. Schlichting, Hermann (J. Kestin, transl.): Boundary-Layer Theory, Seventh ed. McGraw-Hill Book Co., c.1979.
62. Abbott, Ira H.; and Von Doenhoff, Albert E.: Theory of Wing Sections. Dover Publ., Inc., c.1959.
63. Kuo, Ching-Chiang; and Morino, Luigi: Steady Subsonic Flow Around Finite-Thickness Wings. NASA CR-2616, 1975.

64. Jones, R.: The Distribution of Normal Pressures on a Prolate Spheroid. R. & M. No. 1061, British A.R.C., 1925.
65. Van Dyke, Milton: Perturbation Methods in Fluid Mechanics. Parabolic Press, 1975.
66. Gray, R. B.; McMahon, H. M.; Shenoy, K. R.; and Hammer, M. L.: Surface Pressure Measurements at Two Tips of a Model Helicopter Rotor in Hover. NASA CR-3281, 1980.

1. Report No. NASA TP-2197		2. Government Accession No.		3. Recipient's Catalog No.	
4. Title and Subtitle THE COMPRESSIBLE AERODYNAMICS OF ROTATING BLADES BASED ON AN ACOUSTIC FORMULATION				5. Report Date December 1983	
7. Author(s) Lyle N. Long				6. Performing Organization Code 505-42-23-07	
9. Performing Organization Name and Address NASA Langley Research Center Hampton, VA 23665				8. Performing Organization Report No. L-15652	
12. Sponsoring Agency Name and Address National Aeronautics and Space Administration Washington, DC 20546				10. Work Unit No.	
15. Supplementary Notes This report was originally a Ph.D dissertation submitted to The George Washington University, April 25, 1983. F. Farassat (NASA) and M. K. Myers (GWU) directed the dissertation. Editorial revisions have been made.				11. Contract or Grant No.	
16. Abstract In this report, an acoustic formula derived by Farassat for the calculation of the noise of moving bodies is applied to aerodynamic problems. Farassat's acoustic formulation is a time domain result suitable for slender wings and bodies moving at subsonic speeds. The main contribution of this report is the derivation of a singular integral equation in terms of the surface pressure which must then be solved numerically for aerodynamic purposes. However, as the "observer" is moved onto the body surface, the divergent integrals in the acoustic formulation are semiconvergent. The procedure for regularization (or taking principal values of divergent integrals) is explained, and some numerical examples for ellipsoids, wings, and lifting rotors are presented. The numerical results show good agreement with available measured surface pressure data.				13. Type of Report and Period Covered Technical Paper	
17. Key Words (Suggested by Author(s)) Compressible aerodynamics Propeller and rotor loads Acoustics				14. Sponsoring Agency Code	
18. Distribution Statement Unclassified - Unlimited				Subject Category 71	
19. Security Classif. (of this report) Unclassified		20. Security Classif. (of this page) Unclassified		21. No. of Pages 76	
				22. Price A05	

National Aeronautics and
Space Administration

Washington, D.C.
20546

Official Business
Penalty for Private Use, \$300

THIRD-CLASS BULK RATE

Postage and Fees Paid
National Aeronautics and
Space Administration
NASA-451



1 1 10, H, 831208 S00903DS
DEPT OF THE AIR FORCE
AF WEAPONS LABORATORY
ATTN: TECHNICAL LIBRARY (SUL)
KIRTLAND AFB NM 87117

NASA

POSTMASTER: If Undeliverable (Section 158
Postal Manual) Do Not Return